Biogeochemical controls on ammonium accumulation in the surface layer of the Southern Ocean

Shantelle Smith[1*], Katye E. Altieri[1], Mhlangabezi Mdutyana[1,2], David R. Walker[3], Ruan G. Parrott[1], Sedick Gallie[3], Kurt A.M. Spence[1], Jessica M. Burger[1], Sarah E. Fawcett[1,4]

[1] Department of Oceanography, University of Cape Town, Private Bag X3, Rondebosch, Cape Town, South Africa
[2] Southern Ocean Carbon and Climate Observatory (SOCCO), CSIR, Rosebank, Cape Town, South Africa
[3] Department of Conservation and Marine Sciences, Cape Peninsula University of Technology, Cape Town, South Africa
[4] Marine and Antarctic Research centre for Innovation and Sustainability (MARIS), University of Cape Town, Cape Town, South Africa

[*] Corresponding author: smtsha023@myuct.ac.za

1. Abstract

The production and removal of ammonium (NH_4^+) are essential upper-ocean nitrogen cycle pathways, yet in the Southern Ocean where NH_4^+ has been observed to accumulate in surface waters, its mixed-layer cycling remains poorly understood. For surface seawater samples collected between Cape Town and the marginal ice zone in winter 2017, we found that NH_4^+ concentrations were five-fold higher than is typical for summer, and lower north than south of the Subantarctic Front (0.01–0.26 µM versus 0.19–0.70 µM). Our observations confirm that NH_4^+ accumulates in the Southern Ocean's winter mixed layer, particularly in polar waters. NH_4^+ assimilation rates were highest near the Polar Front (12.9 ± 0.4 nM day^{-1}) and in the Subantarctic Zone (10.0 ± 1.5 nM day^{-1}), decreasing towards the marginal ice zone (3.0 ± 0.8 nM day^{-1}) despite the high ambient NH_4^+ concentrations in these southernmost waters, likely due to the low temperatures and limited light availability. By contrast, rates of NH_4^+ oxidation were higher south than north of the Polar Front (16.0 ± 0.8 versus 11.1 ± 0.5 nM day^{-1}), perhaps due to the lower light and higher iron conditions characteristic of polar waters. NH_4^+ concentrations were also measured on five transects of the Southern Ocean (Subtropical- to marginal ice zone) spanning the 2018/2019 annual cycle. These measurements reveal that mixed-layer NH_4^+ accumulation south of the Subantarctic Front derives from sustained heterotrophic NH_4^+ production in late summer through winter that in net, outpaces NH_4^+ removal by temperature-, light-, and iron-limited microorganisms. Our observations thus imply that the Southern Ocean becomes a biological source of CO_2 to the atmosphere for half the year not only because nitrate drawdown is weak, but also because the ambient conditions favour net heterotrophy and NH_4^+ accumulation.

2. Introduction

The Southern Ocean impacts the Earth system through its role in global thermohaline circulation, which drives the exchange of heat and nutrients among ocean basins (Frölicher et al., 2015; Sarmiento et al., 2004). The Southern Ocean also plays an integral role in mediating climate, by

transferring carbon to the deep ocean via its biological and solubility pumps (Sarmiento & Orr, 1991; Volk & Hoffert, 1985) and through the release of deep-ocean CO_2 to the atmosphere during deep-water ventilation (i.e., CO_2 leak; Broecker & Peng, 1992; Lauderdale et al., 2013; Sarmiento & Toggweiler, 1984). Upper Southern Ocean circulation is dominated by the eastward-flowing Antarctic Circumpolar Current (ACC) that consists of a series of broad circumpolar bands ("zones") separated by oceanic fronts. These fronts can drive water mass formation (Ito et al., 2010) and nutrient upwelling that supports elevated productivity (Sokolov & Rintoul, 2007).

Concentrations of the essential macronutrients, nitrate (NO_3^-) and phosphate (PO_4^{3-}), are perennially high in Southern Ocean surface waters, in contrast to most of the global ocean. Assimilation of these nutrients, and thus primary productivity in the Southern Ocean, is limited by numerous overlapping factors, including temperature, light, micronutrient concentrations, and grazing pressure (e.g., Boyd et al., 2001; Martin et al., 1990; Reay et al., 2001; Smith Jr & Lancelot, 2004). The strength of these limitations varies with sector (i.e., longitude), zone (i.e., latitude), and season, resulting in spatial and temporal variability in chlorophyll-a, primary production, plankton community composition, and nutrient uptake regime (Mdutyana et al., 2020; Mengesha et al., 1998; Shadwick et al., 2015; Thomalla et al., 2011). In addition to the seasonality of temperature and light, Southern Ocean ecosystems are influenced by seasonal changes in nutrient availability. In winter, deep mixing replenishes the nutrients required for phytoplankton growth but the low temperatures and light levels impede biological activity (Rintoul & Trull, 2001). Once the mixed layer shoals in spring and summer, phytoplankton consume the available nutrients until some form of limitation (usually iron; Nelson et al., 2001; Nicholson et al., 2019) sets in. This balance between wintertime nutrient recharge and summertime nutrient drawdown is central to the Southern Ocean's role in setting atmospheric CO_2 (Sarmiento & Toggweiler, 1984).

The onset of iron limitation following the spring/early summer bloom in the Southern Ocean drives phytoplankton to increased reliance on recycled ammonium (NH_4^+; Timmermans et al., 1998), the assimilation of which has a far lower iron requirement than that of NO_3^- (Price et al., 1994). The extent to which phytoplankton rely on NO_3^- versus NH_4^+ as their primary N source has implications for Southern Ocean CO_2 removal since phytoplankton growth fuelled by subsurface NO_3^- ("new production") must be balanced on an annual basis by the export of sinking organic matter ("export production"; Dugdale & Goering, 1967), which drives CO_2 sequestration (i.e., the biological pump; Volk & Hoffert, 1985). By contrast, phytoplankton growth on NH_4^+ or other recycled N forms ("regenerated production") yields no net removal of CO_2 to the deep ocean (Dugdale & Goering, 1967). Considerable research has focused on NO_3^- cycling in the Southern Ocean mixed layer because of the importance of this nutrient for the biological pump (e.g., Francois et al., 1992; Johnson et al., 2017; Mdutyana et al., 2020; Primeau et al., 2013; Sarmiento & Toggweiler, 1984) and global ocean fertility (Fripiat et al., 2021; Sarmiento et al., 2004). By contrast, the cycling of regenerated N within the seasonally-varying mixed layer – including the production of NH_4^+ and its removal by phytoplankton and nitrifiers – remains poorly understood.

NH_4^+ is produced in the euphotic zone as a by-product of heterotrophic metabolism (Herbert, 1999) and as a consequence of zooplankton grazing (Lehette et al., 2012; Steinberg & Saba, 2008), and is removed by phytoplankton uptake (in euphotic waters) and nitrification (mainly in

aphotic waters). Heterotrophic bacteria can also consume NH_4^+ (Kirchman, 1994) and have been hypothesized to do so at significant rates in the Southern Ocean mixed layer in winter (Cochlan, 2008; Mdutyana et al., 2020). The assimilation of NH_4^+ by phytoplankton requires relatively little energy (Dortch, 1990) such that NH_4^+ is usually consumed in the euphotic zone as rapidly as it is produced (Glibert, 1982; La Roche, 1983), resulting in very low surface NH_4^+ concentrations in the open ocean (<0.2 μM; Paulot et al., 2015). Additionally, NH_4^+ is often the preferred N source to small phytoplankton (Dortch 1990), which typically dominate when iron and/or light are limiting (Deppeler & Davidson, 2017; Pearce et al., 2010; Tagliabue et al., 2014) since their higher cell surface area-to-volume ratio renders them less vulnerable to diffusion- and/or light limitation (Finkel et al., 2004; Fujiki & Taguchi, 2002; Hudson & Morel, 1993; Mei et al., 2009).

In addition to the implications for size distribution, the dominant N source to phytoplankton is indicative of their potential for CO_2 removal, as per the new production paradigm (Dugdale & Goering, 1967). The N isotopic composition ($\delta^{15}N$, in ‰ vs. N_2 in air, = $(^{15}N/^{14}N_{sample}/^{15}N/^{14}N_{air} - 1) \times 1000$) of particulate organic N (PON; a proxy for phytoplankton biomass) can be used to infer the dominant N source to phytoplankton (Altabet, 1988; Fawcett et al., 2011; Lourey et al., 2003; Van Oostende et al., 2017) since the assimilation of subsurface NO_3^- yields PON that is higher in $\delta^{15}N$ than that fuelled by recycled NH_4^+ uptake (Treibergs et al., 2014). As such, measurements of bulk $\delta^{15}N$-PON can be used to infer the net N uptake regime (Altabet, 1988; Fawcett et al., 2011; 2014; Lourey et al., 2003).

Nitrification, the oxidation of NH_4^+ to nitrite (NO_2^-) and then NO_3^- by chemoautotrophic bacteria and archaea, was historically considered unimportant in euphotic zone waters due to the evidence for light inhibition of nitrifiers (Hooper & Terry, 1974; Horrigan & Springer, 1990; Olson, 1981) and the fact that they are outcompeted by phytoplankton for NH_4^+ (Smith et al., 2014; Ward, 1985; 2005; Zakem et al., 2018). However, this view has been challenged in numerous ocean regions (Yool et al., 2007), including the Southern Ocean (Smart et al., 2015; Cavagna et al., 2015; Fripiat et al., 2015; Mdutyana et al., 2020). Wintertime upper-ocean NH_4^+ dynamics thus have implications for annual estimates of carbon export potential, insofar as NO_3^- produced by nitrification in the winter mixed layer that is subsequently supplied to spring/summer phytoplankton communities constitutes a regenerated rather than a new N source on an annual basis (Mdutyana et al., 2020).

Surface concentrations of NH_4^+ are typically near-zero in spring and early- to mid-summer in the open Southern Ocean (Daly et al., 2001; Henley et al., 2020; Sambrotto & Mace, 2000; Savoye et al., 2004) due to assimilation by phytoplankton. In late summer, a peak in NH_4^+ concentration has been observed and attributed to enhanced bacterial and zooplankton activity following elevated phytoplankton growth (Becquevort et al., 2000; Dennett et al., 2001; Mengesha et al., 1998). The limited available observations suggest that wintertime surface NH_4^+ concentrations are high (often >1 μM), particularly south of the Subantarctic Front (SAF) (Bianchi et al., 1997; Henley et al., 2020; Philibert et al., 2015; Mdutyana et al., 2020; Weir et al., 2020). It thus appears that NH_4^+ is not depleted following the late summer peak in its concentration, which indicates enhanced NH_4^+ regeneration, either coincident with (but in excess of) NH_4^+ assimilation in winter and/or prior to this in late summer and/or autumn. Under these conditions, the Southern Ocean mixed layer may become net heterotrophic and thus a biological source of CO_2 to the atmosphere.

Here, we focus mainly on NH_4^+ cycling in the Southern Ocean mixed layer in winter, a season assumed to be largely biologically dormant (Arrigo et al., 2008; Schaafsma et al., 2018) and for which NH_4^+ cycle data are scarce. We confirm that NH_4^+ accumulates throughout the winter mixed layer south of the SAF, and examine the potential drivers thereof. Using NH_4^+ concentration data collected over a full annual cycle, we propose that these drivers include a contribution from the residual late-summer NH_4^+ pool, sustained NH_4^+ production in the autumn and winter, and limited wintertime NH_4^+ uptake and oxidation that nonetheless exceed the rate of in situ NH_4^+ production. Finally, from our temporally-resolved NH_4^+ concentration data, we propose – for the first time – a measurement-based seasonal cycle for the mixed-layer NH_4^+ pool south of the SAF.

3. Methods

3.1 Cruise tracks and sample collection

Samples were collected for a series of analyses on the southward (S) and northward (N) legs of a winter cruise between Cape Town, South Africa, and the marginal ice zone (MIZ) onboard the R/V *SA Agulhas II* (VOY25; 28 June to 13 July 2017) (Fig. 1). Samples were also collected for NH_4^+ concentration analysis on three cruises onboard the R/V *SA Agulhas II* during 2018/19: early- and late summer samples were collected during the SANAE 58 Relief Voyage (6 December 2018 to 15 March 2019; VOY035); winter samples were collected during the SCALE 2019 (www.scale.org.za) winter cruise to the MIZ (18 July to 12 August 2019; VOY039); and spring samples were collected during the SCALE 2019 spring cruise to the MIZ (12 October to 20 November 2019; VOY040) (Fig. S1).

Leg S of VOY25 in winter 2017 crossed the Atlantic sector and due to logistical constraints, involved only surface underway collections, while leg N bordered the Atlantic and Indian sectors (30°E; WOCE IO6 line) and included eight conductivity-temperature-depth (CTD) hydrocast stations. Frontal positions were determined using the ship's hull-mounted thermosalinograph, supported by temperature, salinity, and oxygen concentration data from CTD measurements made during leg N. The salinity and oxygen sensors were calibrated against seawater samples that were analyzed for salinity using a Portasal 8410A salinometer and for dissolved oxygen by Winkler titration (Strickland & Parsons, 1972). Frontal positions were determined from sharp gradients in potential temperature, salinity, potential density, and oxygen concentrations (Belkin & Gordon, 1996; Lutjeharms & Valentine, 1984; Orsi et al., 1995). For leg N, the mixed layer depth (MLD) was determined for each Niskin (up)cast as the depth between 10 m and 400 m at which the Brunt Väisälä Frequency squared, N^2, reached a maximum (Carvalho et al., 2017).

During leg S, samples were collected every four hours from the ship's underway system (~7 m intake; "underway stations") while samples on leg N were collected from surface Niskin bottles (~10 m, approximately 55% light depth) mounted on the CTD rosette ("CTD stations"). NH_4^+ samples were also taken at 13 depths over the upper 500 m at the CTD stations. At all stations, 40 mL of unfiltered seawater was collected for the analysis of NH_4^+ concentrations in duplicate 50 mL high density polyethylene (HDPE) bottles that had been stored ("aged") with orthophthaldialdehyde (OPA) working reagent. Unfiltered seawater was collected in duplicate

50 mL polypropylene centrifuge tubes for the analysis of NO_3^-, NO_2^-, and PO_4^{3-}, and in a single tube for urea. Immediately following collection, NH_4^+ and nutrient samples were frozen at -20°C.

Duplicate size-fractionated chlorophyll-a samples were collected by filtering seawater (500 mL) through 25 mm-diameter glass fibre filters (0.3 µm and 2.7 µm; Sterlitech GF-75 and Grade D, respectively). Acetone (90%) was added to foil-wrapped borosilicate tubes containing the filters and incubated at -20 °C for 24 hours. Duplicate seawater samples (4 L) were also gently vacuum-filtered through combusted 47 mm-diameter, 0.3 µm GF-75 filters for POC and PON concentrations and δ^{15}N-PON. Filters were stored in combusted foil envelopes at -80°C.

For microscopy, unfiltered seawater samples (250 mL) were collected during leg S in amber glass bottles and immediately fixed by the addition of 2.5 mL of Lugol's iodine solution (2% final concentration), then stored at low room temperature in the dark until analysis. For flow cytometry, seawater samples were collected in triplicate 2 mL microcentrifuge tubes, fixed with glutaraldehyde (1% final concentration), and stored at -80°C until analysis (Marie et al., 2005).

Ten incubation experiments were conducted during leg S to measure net primary production (NPP). In addition, four NPP experiments were conducted during leg N using seawater collected from Niskin bottles fired at ~10 m. In all cases, pre-screened (200-µm mesh; to remove large grazers) seawater was collected in three 2-L polycarbonate bottles to which $NaH^{13}CO_3$ was added at ~5% of the estimated ambient DIC concentration. ^{13}C enrichment was re-calculated post-cruise using measured DIC concentrations, and these enrichments were used in all NPP rate calculations. Bottles were incubated for 5 to 6.5 hours in custom-built deck-board incubators shaded with neutral-density screens to mimic the 55% light level and supplied with running surface seawater. Following incubation, each sample was divided (1 L per size fraction) and gently vacuum filtered through combusted 0.3 µm and 2.7 µm glass fibre filters that were stored in combusted foil at -80°C until analysis.

N uptake (as NO_3^-, NH_4^+ and urea) and NH_4^+ oxidation experiments were conducted at five stations during leg S, with NH_4^+ oxidation measured at two additional stations at the ice edge (Fig. 1). On leg N, experiments were also conducted using seawater collected from ~10 m at the same four CTD stations as the NPP experiments. Duplicate 1 L polycarbonate bottles were amended with ^{15}N-labeled NO_3^-, NH_4^+ or urea at ~10% of the ambient N concentration, estimated based on past wintertime measurements (Mdutyana et al., 2020) and, in the case of NH_4^+, coincident shipboard analyses. ^{15}N enrichment was re-calculated post-cruise using the measured nutrient concentrations, and these enrichments were used in all rate calculations. Incubations were carried out as for NPP. For NH_4^+ oxidation, duplicate black 250 mL HDPE bottles were amended with 0.1 µM $^{15}NH_4^+$ and 0.1 µM $^{14}NO_2^-$ (the latter as a "trap" for the $^{15}NO_2^-$ produced by NH_4^+ oxidation; Ward 2011). NH_4^+ oxidation bottles were incubated for 24 hours under the same temperature conditions as the N uptake and NPP experiments. Subsamples (50 mL) were collected from each bottle immediately following tracer addition (T_0) and at the end of the experiments (T_f), and frozen at -20°C until analysis.

3.2 Sample processing

3.2.1. Ammonium concentrations

On all cruises, NH_4^+ concentrations were measured shipboard using the fluorometric method of Holmes et al. (1999) and a Turner Designs Trilogy fluorometer 7500-000 equipped with a UV module. The detection limit, calculated as twice the pooled standard deviation of all standards, was 0.06 µM. To prevent possible in/efflux of ammonia (NH_3) due to the temperature difference between surface waters and the shipboard laboratory, samples were frozen immediately upon collection, for a maximum of 24 hours. OPA working reagent was added to the frozen samples prior to defrosting them for analysis. Samples were slowly warmed to room temperature in a water bath after OPA addition, incubated in the dark for four hours once defrosted, and then each replicate was measured in triplicate. Standards and blanks were made daily using Type-1 Milli-Q water. Precision was ± 0.03 µM for replicate samples and standards.

During VOY040 (spring 2019), we investigated the possibility that the ship's underway system alters the seawater NH_4^+ concentrations (e.g., due to contamination or cell breakage). We collected surface samples from the underway and Niskin bottles concurrently and measured an average NH_4^+ concentration difference of 0.07 ± 0.15 µM (n=17), with no noticeable trend of one method consistently yielding higher/lower concentrations. We thus have no reason to doubt NH_4^+ concentrations measured for seawater samples collected from the ship's underway system.

3.2.2. Macronutrient concentrations

Following the winter 2017 cruise, duplicate seawater samples were analysed manually for NO_2^- and PO_4^{3-} (Bendschneider & Robinson, 1952; Murphy & Riley, 1962) using a Thermo Scientific Genesys 30 Visible spectrophotometer. Precision and detection limit was ± 0.05 µM and 0.05 µM for NO_2^- and ± 0.06 µM and 0.05 µM for PO_4^{3-}. The concentrations of $NO_3^- + NO_2^-$ and $Si(OH)_4$ were measured using a Lachat QuickChem 8500 Series 2 flow injection autoanalyzer. Aliquots of a certified reference material (JAMSTEC) were measured during each run to ensure measurement accuracy (SD ≤ 2%). The precision of the $NO_3^- + NO_2^-$ and $Si(OH)_4$ measurements was ± 0.4 µM and ± 0.2 µM, respectively, and the detection limit was 0.1 µM and 0.2 µM. NO_3^- concentrations were calculated by subtraction (i.e., $NO_3^- + NO_2^- - NO_2^-$), with error propagated according to standard statistical practices. Urea-N (hereafter, urea) concentrations were determined via the room-temperature, single-reagent colorimetric method (Revilla et al., 2005) using a Thermo Scientific Genesys 30 Visible spectrophotometer; precision was ± 0.04 µM and the detection limit was 0.04 µM.

3.2.3. Chlorophyll-a concentrations

Chlorophyll-a concentrations ([chl-a]) were determined shipboard using the nonacidified fluorometric method (Welschmeyer, 1994). The Turner Designs Trilogy fluorometer was calibrated with an analytical standard (*Anacystis nidulans*, Sigma-Aldrich®) prior to and following the cruise. The [chl-a] of the 0.3-2.7 µm size class (hereafter, "pico" size class) was calculated by subtracting the measured [chl-a] of the >2.7 µm size class (hereafter, "nano+" size class) from the >0.3 µm size class (hereafter, "bulk"). Given previous work showing that the winter Southern Ocean phytoplankton community is composed primarily of small cells (i.e., typically <15 µm; e.g., Hewes et al., 1985; 1990; Weber & El-Sayed, 1987), we did not separate micro- from nanophytoplankton.

3.2.4. Bulk POC, PON and δ^{15}N-PON

The NPP and N uptake filters were fumed with hydrochloric acid in a desiccator for 24 hours to remove inorganic carbon, then dried for 24 hours at 40°C and packaged into tin cups. Filters for δ^{15}N-PON were dried in the same way, but not acidified. Samples were analysed using a Delta V Plus isotope ratio mass spectrometer (IRMS) coupled to a Flash 260 elemental analyser, with a detection limit of 0.17 µmol C and 0.07 µmol N and precision of ±0.005 At% for C and N. Unused pre-combusted filters (blanks) were included in each batch run. POC and PON content was determined from daily standard curves of IRMS area versus known C and N masses. For the isotope ratios, sample measurements were referenced to internal laboratory standards calibrated against IAEA reference materials that were measured after every 5-7 samples.

3.2.5. Size-fractionated rates of NPP and N uptake

Carbon and N uptake rates (NPP, ρNH_4^+, ρNO_3^-, ρUrea) were calculated according to Dugdale & Wilkerson (1986) as:

$$\rho M = \frac{[PM]\ x\ (At\%_{meas} - At\%_{amb})}{T\ x\ (At\%_{init} - At\%_{amb})} \quad \text{(Eqn 1)}$$

$$\text{where, } At\%_{init} = \frac{([M]\ x\ At\%_{amb}) + ([M_{tracer}]\ x\ At\%_{tracer})}{[M] + [M_{tracer}]} \quad \text{(Eqn 2)}$$

Here, M is the species of interest (C, NH_4^+, NO_3^-, or urea); ρM is the uptake rate of that species (nM hour^{-1}, i.e., nmol C or N L^{-1} hour^{-1}); [PM] is the concentration of POC or PON (µM) on the filters; [M] is the ambient concentration of DIC, NH_4^+, NO_3^-, or urea at the time of sample collection; [M_{tracer}] is the concentration of $NaH^{13}CO_3$, $^{15}NH_4^+$, $^{15}NO_3^-$, or ^{15}N-urea added to the incubation bottles; and T is the incubation period (days). DIC concentrations were measured shipboard using a VINDTA 3C instrument and ranged from 2017 to 2130 µM (Bakker et al., 2016). The PM and ρM of the picoplankton size class was calculated by subtracting the nanoplankton from the bulk measurements. Daily rates were computed by multiplying the hourly rates by the number of daylight hours, the latter calculated using the sampling latitude and day of the year (Forsythe et al., 1995).

The f-ratio (Eppley & Peterson, 1979), used to estimate the fraction of NPP potentially available for export, was calculated as:

$$\text{f} - \text{ratio} = \frac{\rho NO_3^-}{\rho N_{tot}} \quad \text{(Eqn 3)}$$

where $\rho N_{tot} = \rho NH_4^+ + \rho NO_3^- +$ ρUrea. Urea uptake was not measured at underway stations 50.7ºS and 55.5ºS (both in the Antarctic Zone); here, the f-ratio was calculated omitting ρUrea. For the two Antarctic Zone stations at which urea uptake was measured, including ρUrea decreased the f-ratio by 8-25% compared to that calculated using only ρNO_3^- and ρNH_4^+.

3.2.6. Ammonia oxidation rates

The azide method (McIlvin and Altabet 2005) was used to convert NO_2^- produced by NH_4^+ oxidation to N_2O gas that was measured using a Delta V Plus IRMS with a custom-built purge-and-trap front end (McIlvin & Casciotti, 2011). This configuration yields a detection limit of 0.2

nmol N with a $\delta^{15}N$ precision of ± 0.1‰. The $\delta^{15}N$ of NO_2^- was derived from $^{45}N_2O/^{44}N_2O$ and the rate of NH_4^+ oxidation ($NH_4^+{}_{ox}$; nM day^{-1}) was calculated following Peng et al. (2015) as:

$$NH_4^+{}_{ox} = \frac{\Delta[^{15}NO_2^-]}{f_{NH_4^+}^{15} \times T} \quad \text{(Eqn 4)}$$

Here, $\Delta[^{15}NO_2^-]$ is the change in the concentration of $^{15}NO_2^-$ (nM) between the start and end of the incubation, calculated as the difference in the measured $\delta^{15}N$ of NO_2^- between the T_f and T_0 samples, $f_{NH_4^+}^{15}$ is the fraction of the NH_4^+ substrate labelled with ^{15}N at the start of the incubation, and T is the incubation length (days). All $^{15}NO_2^-$ produced during the incubations was assumed to derive from $^{15}NH_4^+$ oxidation. The detection limit ranged from 0.02 to 0.11 nM day^{-1}, calculated according to Santoro et al. (2013).

We note that isotope dilution (i.e., the dilution of $^{15}NH_4^+$ by co-occurring $^{14}NH_4^+$ regeneration) during the NH_4^+ uptake and oxidation experiments could potentially lead to an underestimation of the rates (Glibert et al., 1982; Mdutyana, 2021). For the NH_4^+ uptake experiments, their short duration (3 to 7.5 hours) would have rendered the effect of regeneration minor (Mdutyana et al., 2020). Moreover, the $^{15}NH_4^+$ additions were high (100 nM) relative to both the ambient NH_4^+ concentrations north of the SAF and the K_m values derived for NH_4^+ uptake and oxidation in the winter Southern Ocean (150-405 nM and 28-137 nM, respectively; Mdutyana, 2021), making a significant dilution effect unlikely (Lipschultz, 2008). Finally, at the stations south of the SAF, the ambient NH_4^+ concentrations were so high that even if the regeneration of $^{14}NH_4^+$ occurred at an elevated rate (e.g., 50 nM day^{-1}; as has been measured in the late-summer Southern Ocean when remineralization is expected to be high; Goeyens et al., 1991), the $^{15}N/^{14}N$ of the NH_4^+ pool would decrease by <1-2%. We thus consider the potential effect of isotope dilution to be minor.

A further consideration is possible stimulation of the NH_4^+ uptake and oxidation rates by $^{15}NH_4^+$ addition (Lipschultz, 2008). Given the K_m values listed above and the high ambient NH_4^+ concentrations measured in the PFZ and AZ, a stimulation effect could only be significant at the stations north of the SAF where the NH_4^+ concentrations were 10-100 nM, and even then, to a lesser extent for NH_4^+ oxidation than NH_4^+ uptake given that ammonia oxidizers in the winter Southern Ocean become saturated at NH_4^+ concentrations of 100-200 nM (Mdutyana, 2021). The rates reported for the stations north of the SAF should therefore be considered "potential rates." However, since our focus is mainly on explaining the accumulation of NH_4^+ south of the SAF, having "potential" rather than "true" rates for the STZ and SAZ does not affect our conclusions.

3.2.7 Plankton community composition

Microplankton groups (>15 µm) were identified and counted in a subsample (20 mL) from each amber bottle using the Utermöhl technique (Utermöhl, 1958) and following the recommendations of Hasle (1978). Plankton groups and individual species were counted and identified using an inverted light microscope (Olympus CKX41) at 200x magnification. This level of magnification limited the cell sizes that could be reliably distinguished to >15 µm. For each sample, at least 100 cells were enumerated to ensure a statistically valid count.

Pico- and nanoplankton cells (<15 μm) were enumerated using an LSR II flow cytometer (BD Biosciences) equipped with blue, red, violet, and green lasers. Prior to analysis, 1 mL of sample was incubated with 1% (v/v) SYBR Green-I (a DNA stain) at room temperature in the dark for 10 minutes (Marie et al., 1997). From light scatter and autofluorescence, the DNA-containing particles were identified as nano- and picoeukaryotes, and *Synechococcus*. Additionally, small heterotrophic prokaryotes (i.e., bacteria and possibly archaea; hereafter "bacteria") were identified as DNA-containing particles with the lowest detectable autofluorescence (Marie et al., 1997; Gasol & del Giorgio, 2000) (see also Text S2). All particles lacking DNA were considered detritus. The populations of interest were gated using FlowJo 10.3 software (TreeStar, Inc.; www.flowjo.com).

In this study, we did not directly measure NH_4^+ regeneration (i.e., heterotrophy). Instead, we use the abundance of heterotrophic bacteria as a qualitative indicator of NH_4^+ regeneration potential, recognizing that cell abundance does not imply activity. Additionally, we estimate the rate of NH_4^+ production from our concentration and rate data (see section 3.3). The availability of organic matter to heterotrophs is inferred from the abundance of detritus.

3.3 Mixed-layer NH_4^+ residence time and NH_4^+ production rate estimates

The residence time of the mixed-layer NH_4^+ pool can be estimated using the measured ambient NH_4^+ concentrations and corresponding NH_4^+ removal rates as

$$NH_4^+{}_{residence\ time} = \frac{[NH_4^+]}{NH_4^+{}_{removal\ rate}} \quad \text{(Eqn 5)}$$

Here, $NH_4^+{}_{residence\ time}$ is the time period (days) over which a given NH_4^+ concentration will be depleted assuming a constant $NH_4^+{}_{removal\ rate}$. We set $NH_4^+{}_{removal\ rate} = \rho NH_4^+ + NH_4^+{}_{ox}$ in winter and $= \rho NH_4^+$ in late summer given the evidence for negligible mixed-layer NH_4^+ oxidation rates in this latter season (Bianchi et al., 1997; Mdutyana et al., 2020).

To determine the contribution of late summer NH_4^+ production to the wintertime NH_4^+ pool (see section 5.2), we define a rate of NH_4^+concentration decline:

$$NH_4^+{}_{rate\ of\ decline} = NH_4^+{}_{production\ rate} - NH_4^+{}_{removal\ rate} \quad \text{(Eqn 6)}$$

Here, $NH_4^+{}_{production\ rate}$ is the NH_4^+ flux required to compensate for NH_4^+ removal over the late-summer-to-winter period, in order to yield the observed seasonal change in the ambient NH_4^+ concentration.

The rate of NH_4^+concentration decline can also be defined as:

$$NH_4^+{}_{rate\ of\ decline} = \frac{[NH_4^+]_{decline}}{t} \quad \text{(Eqn 7)}$$

Where $[NH_4^+]_{decline}$ is the difference between the late summer and winter NH_4^+ concentrations and t is the time period (days) over which the NH_4^+ concentration declines. Setting Eqn 6 and 7 equal yields:

$$NH_4^+{}_{production\ rate} = \frac{[NH_4^+]_{decline}}{t} + NH_4^+{}_{removal\ rate} \quad \text{(Eqn 8)}$$

Where, $NH_4^+_{consumption\ rate} = \rho NH_4^+ + NH_4^+_{ox}$. Eqns 7 and 8 assume that the elevated wintertime NH_4^+ concentrations result from continuous NH_4^+ production in excess of removal rather than from sporadic events of removal and/or production occurring between late summer and winter.

3.4 Statistical analyses

The correlations among latitude, N concentrations, NPP, N assimilation rates, and NH_4^+ oxidation rates were investigated at the 5% significance level using the Pearson correlation coefficient and the R packages, stats (R Core Team, 2020) and corrplot (Wei & Simko, 2017). Standard deviations were propagated using standard statistical practices.

4. Results

4.1 Hydrography

Sea surface temperature (SST) decreased by ~17 °C between Cape Town (~34°S) and the edge of the MIZ (61.7°S), with similar gradients measured for legs S and N. During leg N, fairly deep MLDs were observed (124-212 m), similar to June and July climatological MLDs compiled from Argo float data for this region (Dong et al., 2008). While the focus of this study is the surface (i.e., upper ~10 m), we report the MLDs here to show that sampling took place under typical winter conditions, with the deep MLDs evincing ongoing winter mixing and associated nutrient recharge. Where not specified, the trends discussed below refer to the surface data only. Latitudinal variations in each parameter are assessed by comparing the various Southern Ocean zones – the Subtropical Zone (STZ) north of the Subtropical Front (STF), the Subantarctic Zone (SAZ) between the STF and the Subantarctic Front (SAF), the Polar Frontal Zone (PFZ) between the SAF and the Polar Front (PF), and south of the PF, the Open and Polar Antarctic Zones (OAZ and PAZ, which are divided by the Southern Antarctic Circumpolar Current Front (SACCF) and collectively termed the Antarctic Zone (AZ); see Text S1 for detailed definitions of the fronts and zones, and Fig. 1 and S1 for their positions at the time of sampling). For each parameter, the average ± 1 standard deviation (SD) for each Southern Ocean zone is reported in Table 1.

4.2 Macronutrient concentrations

In winter 2017, the surface and mixed-layer concentrations of NH_4^+ ranged from below detection to 0.70 μM (Fig. 2a and b). Surface concentrations were higher in the PFZ, OAZ, and PAZ (0.42 ± 0.01 μM, 0.52 ± 0.01 μM, and 0.58 ± 0.01 μM, respectively) than in the STZ and SAZ (0.08 ± 0.03 μM and 0.06 ± 0.01 μM, respectively), with a sharp gradient observed at the SAF. South of the SAF, high NH_4^+ concentrations persisted near-homogeneously throughout the mixed layer, with mixed layer averages ranging from 0.65 ± 0.01 μM at station 58.5°S to 0.27 ± 0.01 μM at station 48.0°S and averaging 0.47 ± 0.02 μM, with concentrations that were below detection north of the SAF (Fig. 2b). Below the mixed layer, NH_4^+ concentrations decreased rapidly at all stations to values below detection by 200 m.

The concentrations of NO_3^- and PO_4^{3-} increased southwards from <10 μM and <1 μM in the STZ to >20 μM and >1.5 μM in the PFZ, OAZ, and PAZ (Fig. 2c and S3a), with the sharpest gradients occurring near the SAF. The concentrations of $Si(OH)_4$ increased rapidly across the PF, from an average of 3.2 ± 1.1 μM between 35.0°S and 48.0°S to 45.6 ± 0.6 μM between 52.1°S and 58.9°S

(Fig. S3b). The NO_2^- concentrations were consistently low across the transect (0.16 ± 0.02 µM; Fig. S3c), as were the concentrations of urea (0.20 ± 0.04 µM; Table 1), with slightly lower urea concentrations observed in the SAZ than in the other zones.

4.3 Chlorophyll-a, POC and PON

The highest bulk [chl-a] was observed near the South African continental shelf, decreasing across the STF and remaining low thereafter (Fig. 3a). The proportion of chl-a in the nano+ size class varied across the region but was >50% at all stations, with higher (>80%) contributions near the fronts and at many OAZ and PAZ stations (Fig. 3b). The nano+ contribution was ≤60% at only five stations (three in the SAZ, two in the OAZ).

The concentrations of bulk POC and PON were highest north of the STF and slightly higher in the OAZ than in the SAZ and PFZ (Fig. S4a and b). The contribution of the nano+ size fraction to POC and PON across the transect was 77.1 ± 22.6% and 66.9 ± 24.2%, respectively (Fig. S4c and d). The δ^{15}N-PON decreased southwards from the STZ and SAZ (1.7 ± 1.0‰) to the PFZ and OAZ (0.5 ± 0.5‰; Fig. 4). Despite considerable differences among zones, the δ^{15}N-PON was relatively homogenous within each zone.

4.4 Rates of net primary production, nitrogen uptake, and ammonium oxidation

Rates of bulk NPP were two- to six-fold higher in the SAZ and PFZ than has been reported previously for the Atlantic sector in winter (Mdutyana et al., 2020; Froneman et al., 1999) (Fig. 5a). By contrast, NPP was low in the OAZ, consistent with previous measurements (Kottmeier & Sullivan, 1987; Mdutyana et al., 2020). The relative contribution of the nano+ size class generally decreased southwards, from 85.4% at 37.0°S to 24.4% at 53.5°S, before increasing to >80% near the SACCF.

The bulk NH_4^+ uptake rates (ρNH_4^+) generally increased southwards from the STZ to the SAZ and PFZ, and then decreased across the OAZ to reach a minimum at the southernmost station (Fig. 5b). In the nano+ size fraction, ρNH_4^+ changed little latitudinally, although it was slightly lower in the PFZ than in the other zones. The contribution of nanoplankton to ρNH_4^+ ranged from 32.8% in the PFZ to 71.9% in the STZ. The bulk NO_3^- uptake rates (ρNO_3^-) were also low in the STZ, while the highest ρNO_3^- was measured in the SAZ, with the rate then decreasing southwards. ρNO_3^- in the nano+ size class followed the same trend as total community ρNO_3^-, with the nanoplankton accounting for 71.5 ± 0.3% of bulk ρNO_3^- on average. The rates of bulk urea uptake (ρUrea) were highest in the STZ, with the SAZ and the PFZ hosting similar rates, and the lowest rates were measured in the OAZ. ρUrea for the nano+ size class followed a similar trend to bulk ρUrea, and nanoplankton accounted for 51.8% of ρUrea in the SAZ, increasing to 100% in the PAZ. The uptake rates of the different N forms were not significantly correlated with one another or with the ambient N concentrations (Table S1).

Ammonium oxidation rates ($NH_4^+{}_{ox}$) increased southwards, with higher $NH_4^+{}_{ox}$ in the OAZ and PAZ than in the STZ, SAZ, and PFZ (Fig. 5c). $NH_4^+{}_{ox}$ was generally comparable to previous wintertime measurements from the surface of the open Southern Ocean (Mdutyana et al., 2020). $NH_4^+{}_{ox}$ was not correlated with the ambient NH_4^+ concentration (Table S1).

435 4.5 Plankton community composition

436 Microplankton abundance was low, with the highest cell counts recorded at stations 37.2°S and
437 41.3°S in the STZ and no cells counted at 38.1°S (STZ) and 55.5°S (OAZ) (Fig. 6a). On average,
438 microplankton abundance was higher in the STZ than in the SAZ, PFZ, and OAZ. The greatest
439 diversity of microplankton groups was observed at 41.3°S in the STZ and at 50.0°S near the PF.

440 Centric diatoms (including *Planktoniella*, *Coscinodiscus*, and *Thalassiosira* species) were
441 detected only at the southernmost station 58.9°S (3 cells mL^{-1}). Pennate diatoms (including
442 *Pseudo-nitzschia*, *Pleurosigma*, and *Navicula* species) were more abundant in the STZ, PFZ, and
443 OAZ, with negligible abundances in the SAZ. Higher pennate diatom abundances occurred near
444 the PF (7 cells mL^{-1}), as has been observed in summer (e.g., Bracher et al., 1999). Dinoflagellates
445 were identified at every station except 38.1°S and were most abundant in the STZ and PFZ. At
446 all but three stations, small (~15 μm) dinoflagellates were the most abundant group, although the
447 larger *Protoperidinium* dinoflagellate species (mainly heterotrophic; Jeong & Latz, 1994) were
448 almost as abundant in the PFZ and at 54.0°S. Microzooplankton (i.e., ciliates, 20-200 μm) were
449 most abundant in the STZ, and were also present in the PFZ at 46.1°S (3 cells mL^{-1}) and 48.9°S
450 (3 cells mL^{-1}) and in the OAZ at 50.0°S (1 cells mL^{-1}) and 54.0°S (4 cells mL^{-1}). All other
451 stations were characterized by negligible (<1 cells mL^{-1}) microzooplankton abundances.

452 Nano- and picoeukaryotes, *Synechococcus*, and heterotrophic bacteria (collectively, "small
453 cells") were roughly 10^3-times more abundant than the microplankton (Fig. 6b). Notwithstanding
454 a lack of data from the STZ, the highest small cell abundances occurred in the SAZ near the SAF.
455 Across the transect, picoeukaryotes were generally more abundant than all other phytoplankton
456 groups (average picoeukaryote contribution to total small cells of 12-54%; nanoeukaryotes of 7-
457 39%; *Synechococcus* of 15-42%). A similar trend has been observed for the Southern Ocean in
458 spring (Detmer & Bathmann, 1997) and late summer (Fiala et al., 1998), in contrast to mid-
459 summer observations showing nanoplankton dominance (e.g., Ishikawa et al., 2002; Weber &
460 El-Sayed, 1987). Additionally, picoeukaryotes were two- to three orders of magnitude more
461 abundant in the SAZ and PFZ than in the OAZ. Nanoeukaryotes dominated near the PF at 50.0°S
462 (39%) and in the southern OAZ at 55.5°S (36%), while *Synechococcus* dominated at 42.7°S and
463 54.0°S (42% and 33%, respectively). In general, nanoeukaryote abundance was higher in the
464 SAZ than in the PFZ and OAZ, as was that of *Synechococcus*.

465 The contribution of heterotrophic bacteria to total small cells varied considerably (10-62%),
466 reaching a maximum south of the PF at 53.0°S and 57.8°S (62% and 50%), and with higher
467 abundances in the SAZ than in the PFZ and OAZ (Fig. 7). Additionally, heterotrophic bacterial
468 abundances were ten-fold lower to two-fold higher than the total pico- and nanophytoplankton
469 cell counts. Detrital particles were most abundant near the southern edge of the SAF, and were
470 generally more abundant in the PFZ than in the SAZ and OAZ (Fig. S5).

471 4.6 2018/19 cruises: ammonium concentrations

472 In early summer, surface NH_4^+ concentrations were uniformly low across the transect (average
473 of 0.11 ± 0.09 μM; Fig. 8a). South of the SAF, NH_4^+ increased to an average concentration of
474 0.81 ± 0.92 μM by late summer (Fig. 8b). By winter 2019, the NH_4^+ concentrations south of the
475 SAF were ~40% lower than they had been in late summer (Fig. 8c), and were similar to those

observed in winter 2017 (0.50 ± 0.30 μM and 0.52 ± 0.11 μM, respectively), confirming that our 2017 observations are generally representative of the wintertime Southern Ocean. By early spring, the NH_4^+ concentrations south of the SAF had declined to near or below detection (0.09 ± 0.08 μM; Fig. 8d) before rising again by late spring to an average value only slightly lower than that measured in winter (0.40 ± 0.74 μM; Fig. 8e). However, the late-spring NH_4^+ concentrations were only elevated in the PFZ (range of 0.11 ± 0.01 to 4.39 ± 0.03 μM, average of 0.77 ± 1.11 μM), as has been observed previously (Bathmann et al., 1997). Excluding the PFZ data yields a far lower late-spring average of 0.17 ± 0.11 μM south of the SAF, which we take as more broadly representative of this season.

4.7 Mixed-layer NH_4^+ residence time and NH_4^+ production rate estimates

The $NH_4^+{}_{\text{residence time}}$ in winter 2017 south of the SAF, computed using Eqn 5, ranged from 10 to 38 days (median of 21 days). These values were estimated using wintertime measurements only and as such, may not be representative of the transition from summer to winter. To refine our estimates, we use the average ρNH_4^+ and NH_4^+ concentration measured south of the SAF in late summer (50.6 ± 24.0 nM day^{-1} and 0.81 ± 0.92 μM, respectively; Deary, 2020), which yields an $NH_4^+{}_{\text{residence time}}$ of 2 to 27 days (median of 5 days).

The $NH_4^+{}_{\text{production rate}}$, calculated using Eqn 8 and an $[NH_4^+]_{\text{decline}}$ of 330 nM (i.e., 810 nM – 480 nM), t of 141 days, and $NH_4^+{}_{\text{removal rate}}$ of 50.6 ± 24.0 nM day^{-1} (here, the average late-summer ρNH_4^+ south of the SAF is used to approximate $NH_4^+{}_{\text{removal rate}}$), was 52.9 ± 25.0 nM day^{-1}. If we instead use the average $NH_4^+{}_{\text{removal rate}}$ and NH_4^+ concentration measured in winter 2017 (21.4 ± 0.6 nM day^{-1} and 520 ± 110 nM), the $NH_4^+{}_{\text{production rate}}$ was 23.4 ± 6.6 nM day^{-1}. Using the range of $NH_4^+{}_{\text{removal rate}}$ values and the average ambient NH_4^+ concentration measured south of the SAF in winter 2017 (16.7 to 31.2 nM day^{-1} and 520 nM) and late summer 2019 (22.6 to 98.6 nM day^{-1} and 810 nM), we calculate that over the late-summer-to-winter transition, the $NH_4^+{}_{\text{production rate}}$ ranged from 18.8 to 100.9 nM day^{-1}.

5. Discussion

5.1 Drivers of NH_4^+ cycling in the surface layer of the Southern Ocean

Previous work has suggested that NH_4^+ accumulates in the Southern Ocean mixed layer following the late summer increase in heterotrophy, then decreases into autumn as heterotrophic activity subsides, to be depleted by winter due to advective processes and biological removal (Koike et al., 1986; Serebrennikova & Fanning, 2004). However, our data show that NH_4^+ concentrations are elevated in the mixed layer in winter, particularly south of the SAF (Fig. 2). Similarly elevated winter surface-layer NH_4^+ has been observed previously in both the Atlantic and Indian sectors, with concentrations typically increasing towards the south (Philibert et al., 2015; Mdutyana et al., 2020; Bianchi et al., 1997). Numerous overlapping processes are likely involved in setting the ambient NH_4^+ concentrations, as summarized in Fig. 9. In this study, we directly measured the rates of NH_4^+ uptake and oxidation, and estimated the rates of NH_4^+ production, along with qualitatively evaluating heterotrophy from the relative abundance of heterotrophic bacteria, phytoplankton, and detritus. For the NH_4^+ cycle processes shown in Fig. 9 that are not quantified or inferred from our dataset, we consider their potential role in Southern Ocean NH_4^+ cycling based on findings reported in the literature.

The high NH_4^+ concentrations observed south of the SAF in winter may result from net NH_4^+ accumulation during late summer, autumn, and/or winter. The persistence of elevated NH_4^+ concentrations that are near-homogeneously distributed throughout the mixed layer is consistent with a residence time for the winter NH_4^+ reservoir in excess of the time-scale for upper-ocean mixing. Indeed, we calculate a median residence time of 21 days south of the SAF, compared to 2 days north of the SAF. One implication of the long residence time computed for the polar zones is that the wintertime NH_4^+ pool likely reflects both ongoing processes and those that occurred earlier in the year. We posit that the elevated NH_4^+ concentrations south of the SAF may result from higher wintertime rates of NH_4^+ production than removal and/or from the gradual but incomplete depletion in winter of NH_4^+ produced mainly in late summer and autumn. We evaluate both possibilities throughout the discussion below.

5.1.1 Ammonium removal

Ammonium assimilation – Microbial growth is limited in the winter Southern Ocean (Arrigo et al., 2008; Smith Jr et al., 2000, Takao et al., 2012), resulting in low cell abundances and nutrient uptake rates (Church et al., 2003; Iida & Odate, 2014; Mdutyana et al., 2020). However, while the concentrations of chl-a and rates of NPP were low across our transect, they were not negligible (Fig. 3a and 5a), consistent with previous reports for this season (Mordy et al., 1995; Pomeroy & Wiebe, 2001). Southern Ocean phytoplankton are adapted to survive suboptimal conditions; for example, numerous species achieve their maximum growth rates at temperatures that are considerably lower than the optimal growth temperatures of temperate and tropical species (2-9 °C versus 10-30 °C and 15-35 °C, respectively), with sharp declines in growth rates observed at temperatures outside this range (Boyd et al., 2013; Coello-Camba & Agusti, 2017; Fiala & Oriol, 1990). In addition, ice-free Southern Ocean waters typically extend to <60°S in the eastern Atlantic and western Indian sectors in winter, so that even though irradiance levels may not be optimal for phytoplankton growth, there is always some light available for photosynthesis. The hostile wintertime conditions of the open Southern Ocean do not, therefore, prevent ecosystem functioning, although the microbial dynamics and associated biogeochemical processes differ from those occurring in summer (Smart et al., 2015; Mdutyana et al., 2020).

We measured fairly low surface NH_4^+ uptake rates (3.0-13.2 nM day^{-1}; Fig. 5b) compared to previous wintertime observations (ranging from 32-66 nM day^{-1}; Cota et al., 1992; Mdutyana et al., 2020; Philibert et al., 2015). Such low rates, if generally representative of winter, would limit mixed-layer NH_4^+ drawdown, especially south of the PF where ρNH_4^+ was particularly low. Recycled N (NH_4^+ + urea) nonetheless accounted for most of the N assimilated during winter, including in the AZ (Fig. 5b).

The available δ^{15}N-PON data suggest that the preferential reliance of phytoplankton on recycled N may have persisted from the late summer. In theory, PON generated in early- through mid-summer from the assimilation of upwelled NO_3^- (δ^{15}N-NO_3^- of 5.2‰ in the AZ and 6.2‰ in the SAZ; Smart et al., 2015; Fripiat et al., 2019; 2021) will have a δ^{15}N of ~0‰ in the AZ and 1-2‰ in the SAZ given the isotope effect of NO_3^- assimilation and the degree of seasonal NO_3^- drawdown (Sigman et al., 1999; Granger et al., 2004; 2010). Such δ^{15}N-PON values have indeed been measured in the early- and mid-summer Southern Ocean (Lourey et al., 2003; Smart et al., 2020; Soares et al., 2015). By late summer, δ^{15}N-PON has been observed to decline to between

-5 and -1‰, with the lowest values occurring in the AZ (Lourey et al., 2003; Smart et al., 2020; Trull et al., 2008). Since the $\delta^{15}N$ of recycled N is expected to be low (<0‰; Checkley & Miller, 1989, Macko et al., 1986), the early-to-late summer decline in $\delta^{15}N$-PON implicates a switch from dominantly NO_3^-- to dominantly recycled N-supported phytoplankton growth (Lourey et al., 2003). For the SAZ, the subsequent late summer-to-winter rise in $\delta^{15}N$-PON (i.e., from ~ -1‰ to 1-2.5‰; Fig. 4) has previously been attributed to PON decomposition by heterotrophic bacteria (Smart et al., 2020), during which ^{14}N-NH_4^+ is preferentially remineralized, leaving the remaining PON enriched in ^{15}N (Möbius, 2013). That NH_4^+ concentrations are not elevated in the SAZ mixed layer in winter (Fig. 2b) indicates that the remineralized NH_4^+ is rapidly re-assimilated by phytoplankton and/or oxidized to NO_2^- in this zone. In the AZ, the much lower $\delta^{15}N$-PON of -3 to -1‰ that we observe in winter surface waters requires the sustained assimilation of low-$\delta^{15}N$ N (i.e., recycled N) to offset a remineralization-driven $\delta^{15}N$ rise akin to that of the SAZ. We conclude that Southern Ocean phytoplankton preferentially consume regenerated N from late summer until at least July (albeit at low rates in winter), particularly south of the PF.

The fact that NH_4^+ accumulated in the winter mixed layer despite being the preferred phytoplankton N source in late summer through winter implies that low rates of NH_4^+ uptake contributed to its accumulation. Multiple factors may cause low rates of photoautotrophic NH_4^+ assimilation, including deplete NH_4^+ and micronutrient concentrations, light limitation, and low temperatures. North of the SAF, NH_4^+ concentrations below detection likely limited ρNH_4^+, as evidenced by the fact that in a series of experiments conducted on the same cruise, ρNH_4^+ increased with the addition of NH_4^+ at these stations (Mdutyana, 2021). By contrast, south of the SAF, NH_4^+ concentrations were similar to or higher than the half-saturation constant (K_m) derived for NH_4^+ uptake in the winter Southern Ocean (0.2 to 0.4 µM; Mdutyana, 2021), suggesting that something other than NH_4^+ availability was limiting to phytoplankton at these latitudes.

Iron is not directly involved in NH_4^+ assimilation but is required for electron transport during photosynthesis and respiration (Raven, 1988). While iron limitation is widespread across the Southern Ocean (Janssen et al., 2020; Pausch et al., 2019; Viljoen et al., 2019), iron availability appears to be higher in winter than during other seasons (Mtshali et al., 2019; Tagliabue et al., 2014) due to enhanced mixing, storms, and increased aeolian deposition (Coale et al., 2005; Honjo et al., 2000; Sedwick et al., 2008). The fact that ρNO_3^- and ρNH_4^+ were generally similar across the transect (Fig. 5b) argues against a dominant role for iron in controlling ρNH_4^+ since NO_3^- assimilation has a far higher iron requirement than NH_4^+ assimilation (Morel et al., 1991).

In contrast to NH_4^+ and iron availability, light limitation is exacerbated in winter due to low insolation, increased cloud-cover, and mixed layers that can be hundreds of meters deeper than the euphotic zone (Buongiorno Nardelli et al., 2017; Sallée et al., 2010). Light is thus often considered the dominant constraint on Southern Ocean primary productivity in this season (Thomalla et al., 2011; Llort et al., 2019; Wadley et al., 2014). However, since NH_4^+ assimilation by phytoplankton is fairly energetically inexpensive (Dortch, 1990), it should occur even under low light conditions (recognizing that light remains critical for coincident CO_2 fixation). Heterotrophic bacteria can also consume NH_4^+ (Kirchman, 1994), including in the dark, as they derive energy from organic carbon oxidation rather than light. At an ecosystem level, therefore,

NH_4^+ assimilation may not be primarily limited by light, although this parameter clearly strongly controls the rate and distribution of NPP (Fig. 5a).

Previous observations suggest that temperature can influence NH_4^+ uptake, especially in winter (Glibert, 1982; Reay et al., 2001). The negative effect of temperature appears to be enhanced under high-nutrient and low-light conditions, at least in the case of phytoplankton growth rates (Baird et al., 2001). Experiments conducted coincident with our sampling showed that the maximum rate of NH_4^+ uptake (V_{max}) achievable by the *in situ* community was strongly negatively correlated with temperature and latitude (Mdutyana, 2021), with the latter parameter representing the combined role of light, temperature, and possibly iron, the average concentration of which appears to increase from the SAZ to the AZ (Tagliabue et al., 2012). We conclude that these three drivers, along with NH_4^+ availability north of the SAF, may all play a role in controlling photoautotrophic NH_4^+ assimilation in the winter Southern Ocean, with complex interactions among them that are difficult to disentangle.

In addition to physical and chemical limitations, microbial preference for other N species may impact NH_4^+ depletion. For example, the preferential uptake of urea and/or other dissolved organic N (DON) species by some organisms (e.g., picoeukaryotes, cyano- or heterotrophic bacteria) could cause a net decrease in the total NH_4^+ uptake rates. While urea has been shown to constitute a large fraction of the total N assimilated by Southern Ocean phytoplankton in summer and autumn (albeit mainly in the SAZ; Joubert et al., 2011; Thomalla et al., 2011), we measured fairly low ρUrea (Fig. 5b), which is perhaps unsurprising given the low ambient urea concentrations (Table 1). The exceptions were stations 37°S and 43.0°S where ρUrea was higher than ρNH_4^+, coincident with very low ambient NH_4^+ (0.10 µM and below detection) and relatively high urea concentrations (0.36 µM and 0.15 µM).

Community composition can also alter the N uptake regime. Small phytoplankton, such as the numerically-dominant nano- and picoeukaryotes, are more likely to consume NH_4^+ and urea than NO_3^- (Koike et al., 1986; Lee et al., 2012; 2013), especially under conditions of severe iron and light limitation (Sunda & Huntsman, 1997). Across our transect, reduced N (i.e., NH_4^+ + urea) uptake exceeded NO_3^- uptake for both the total phytoplankton community (transect average of 12.0 ± 0.9 nM day^{-1} for reduced N versus 5.8 ± 1.0 nM day^{-1} for NO_3^-; f-ratio of 0.36) and the pico size fraction (5.0 ± 1.2 nM day^{-1} versus 1.9 ± 1.2 nM day^{-1}; f-ratio of 0.27; Fig. 5b). That said, the NO_3^- uptake rates were not negligible, including in the pico size fraction. In the PFZ and AZ, NO_3^- uptake by the picoplankton was far more strongly correlated with the abundance of picoeukaryotes than *Synechococcus* (r = 0.75 and 0.03, respectively), consistent with observations of dominant reliance on NO_3^- by picoeukaryotes and NH_4^+ by *Synechococcus* in other ocean regions (Fawcett et al., 2011; 2014; Painter et al., 2014). Additionally, *Synechococcus* abundance was strongly correlated with NH_4^+ concentration south of the SAF (r = 0.65). In the nano+ size class, NO_3^- uptake was likely driven in the SAZ by dinoflagellates and nanoeukaryotes, and in the PFZ and AZ by diatoms, which remain active in these zones in winter (Weir et al., 2020). By contrast, nanoeukaryotes, which have a higher per-cell nutrient requirement than the equally-abundant picoeukaryotes, may have dominated NH_4^+ uptake in the PFZ and AZ given that higher nanoeukaryote abundances corresponded with lower NH_4^+ concentrations at a number of stations (e.g., stations 50.0°S, 51.1°S, and 55.5°S; Fig. 6b).

The low abundances of diatoms and dinoflagellates and absence of coccolithophores across our transect (Fig. 6a) is expected given the limitations imposed on nutrient uptake and CO_2 fixation by winter Southern Ocean conditions. The lower surface area-to-volume ratio of large cells means that they rapidly experience diffusion-limitation of NH_4^+ and micronutrient uptake and are more susceptible to light limitation (Finkel et al., 2004), resulting in their being outcompeted by smaller species for essential resources (Franck et al., 2005; Cavender-Bares et al., 1999). The near-absence of centric diatoms is also best explained thus, particularly given their low surface area-to-volume ratio compared to the more-abundant pennate species (Kobayashi & Takahashi, 2002) that are more likely to consume NH_4^+ (Semeneh et al., 1998). Diatom success in winter may also be limited by enhanced mixing, as this group generally prefers stratified waters (Kopczynska et al., 2007).

In sum, NH_4^+ uptake rates were low across our transect but not negligible, indicating that phytoplankton activity in winter, which is dominated by smaller species, is a sink for NH_4^+. The hostile conditions of the winter Southern Ocean imposed limitations on NH_4^+ uptake that varied with latitude, with NH_4^+ concentrations controlling ρNH_4^+ north of the SAF, while light and temperature were important south of the SAF. Additionally, *Synechococcus,* nanoeukaryotes, and pennate diatoms likely dominated NH_4^+ assimilation, consistent with previous observations from the Southern Ocean and elsewhere (Klawonn et al., 2019; Semeneh et al., 1998).

Ammonium oxidation – Nitrification removes more mixed-layer NH_4^+ in winter than phytoplankton assimilation south of the PF, with NH_4^+ oxidation rates that were two- to five-times the co-occurring NH_4^+ uptake rates (Fig. 5c). The comparative success of ammonia oxidisers may be due to decreased competition with phytoplankton for NH_4^+, augmented by decreased photoinhibition (Wan et al., 2018; Lu et al., 2020), elevated NH_4^+ availability (Baer et al., 2014; Mdutyana et al., 2020; Mdutyana, 2021), and the minimal effect of temperature on NH_4^+ oxidation (Bianchi et al., 1997; Baer et al., 2014; Horak et al., 2013; Mdutyana 2021). One implication of the dominance of NH_4^+ oxidation in winter is that in addition to the limitations on photoautotrophic NH_4^+ assimilation discussed above, low phytoplankton success in the AZ may result from nitrifiers outcompeting phytoplankton for scarce resources (e.g., trace elements required for enzyme functioning, such as iron and copper; Amin et al., 2013; Maldonado et al., 2006; Shafiee et al., 2019) under conditions of low incident light and enhanced mixing.

The K_m derived for NH_4^+ oxidation in the winter Southern Ocean has recently been reported to be low (0.03 to 0.14 μM), with ammonia oxidizers observed to become saturated at ambient NH_4^+ concentrations of ~0.1-0.2 μM (Mdutyana, 2021). This means that south of the SAF in winter 2017, ammonia oxidizers were not substrate limited (as implied by the lack of correlation between $NH_4^+{}_{ox}$ and NH_4^+ concentration; Table S1), which raises the question of why NH_4^+ oxidation did not occur at higher rates. The answer may indirectly involve temperature, in that psychrophilic organisms can be less responsive to high substrate concentrations at low temperatures (Baer et al., 2014). Another possibility is that NH_4^+ oxidation was iron-limited (Shiozaki et al., 2016; Shafiee et al., 2019; Mdutyana, 2021). In any case, ammonia oxidisers were moderately successful across the surface Southern Ocean in winter, with low light, reduced competition with phytoplankton, and substrate repletion likely explaining the elevated NH_4^+ oxidation rates south of the PF compared to the stations to the north.

686 5.1.2 Ammonium production and other sources of ammonium

687 NH_4^+ production must have been sustained during the winter to maintain a mixed-layer NH_4^+
688 pool south of the SAF that was high in concentration relative to the early summer. Indeed, the
689 residence time estimated for NH_4^+ in winter (10 to 38 days) is considerably shorter than the
690 transition from late summer to winter (approximately three months), indicating that heterotrophic
691 NH_4^+ production, which would have occurred coincident with NH_4^+ consumption, must have
692 been ongoing in winter. We estimate the rate of this wintertime NH_4^+ production to be 23.4 ± 6.6
693 nM day^{-1}.

694 *Heterotrophic activity by bacteria* – Heterotrophic bacteria contribute significantly to NH_4^+
695 production in the Southern Ocean (Hewes et al., 1985; Koike et al., 1986; Tréguer & Jacques,
696 1992), including in winter (Rembauville et al., 2017). In our dataset, lower ratios of
697 photosynthetic-to-heterotrophic cells were observed at stations with higher NH_4^+ concentrations
698 (e.g., stations 48.9°S, 53.0°S, 54.0°S, and 57.8°S; Fig.7a), consistent with a role for the
699 heterotrophic bacteria present at the time of sampling in generating the ambient NH_4^+ pool. The
700 potential for ongoing heterotrophic activity can also be inferred from the high detrital particle
701 counts along the transect (Fig. 7b). However, since heterotrophic bacteria are likely more active
702 in late summer and autumn when the temperature and the supply of labile PON are higher
703 (Becquevort et al., 2000; Dennett et al., 2001; Pomeroy & Wiebe, 2001; Smart et al., 2020), we
704 expect that the winter NH_4^+ pool includes NH_4^+ produced in late summer and autumn. A further
705 consideration is assimilation of NH_4^+ by heterotrophic bacteria, reported to occur at elevated
706 rates in the Southern Ocean mixed layer in winter (Mdutyana et al. 2020; Text S3). If this process
707 is a persistent feature of the winter Southern Ocean, it will decrease the net contribution of
708 heterotrophic bacteria to NH_4^+ accumulation. We conclude that it is unlikely that the surface NH_4^+
709 pool measured in winter derived solely from wintertime bacterial NH_4^+ production given that yet
710 higher NH_4^+ concentrations have been observed in late summer and autumn (Becquevort et al.,
711 2000; Dennett et al., 2001), including in the present study (see section 5.2 below).

712 *Heterotrophic activity by zooplankton* – While the microzooplankton enumerated in this study
713 occurred at very low abundances, those that were present likely contributed to the NH_4^+ flux. For
714 example, at stations 48.9°S and 54.0°S in the PFZ and AZ, respectively, both the ratios of
715 photosynthetic-to-heterotrophic cells and the absolute abundances of heterotrophic bacteria were
716 low, while the microzooplankton abundances and NH_4^+ concentrations were elevated compared
717 to nearby stations. The implication of these observations is that elevated microzooplankton
718 abundances may help to explain high NH_4^+ concentrations in waters with low numbers of
719 heterotrophic bacteria, although we note that this scenario only occurred at two stations. On
720 balance, we posit that microzooplankton are less important for wintertime NH_4^+ production than
721 heterotrophic bacteria given their low abundances in the surface layer (Fig. 6a; Atkinson et al.,
722 2012).

723 Above, we have assumed that NH_4^+ production is the direct result of heterotrophy. However,
724 there are other possible mechanisms of NH_4^+ supply that should be considered. We briefly
725 address some of these processes below, noting that for most, there are very few to no observations
726 available from the Southern Ocean.

DON cycling – NH_4^+ can be released by heterotrophic bacteria that directly consume DON (e.g., urea; Billen, 1983; Tupas & Koike, 1990), and possibly also by ammonia oxidisers that convert DON to NH_4^+ intracellularly, through the equilibration of the intra- and extracellular NH_4^+ pools (Kitzinger et al., 2019). DON can also be converted to NH_4^+ through photodegradation by UV radiation (e.g., Aarnos et al., 2012). Bacterial decomposition of DON (rather than PON) to NH_4^+ is implicit in most estimates of ammonification, however, and cellular NH_4^+ efflux by ammonia oxidisers is likely extremely low given that they require NH_4^+ to fix CO_2. Additionally, the low light flux to the surface Southern Ocean in winter means that photodegradation will not yield a significant supply of NH_4^+. Thus, DON conversion to NH_4^+, through any mechanism, is probably negligible.

External inputs of ammonium – High surface ocean NH_4^+ concentrations may theoretically derive from external inputs of NH_4^+, such as N_2 fixation, NH_4^+ aerosol deposition, or sea-ice melt. N_2 fixation should be below detection in the winter Southern Ocean due to the cold temperatures, low light and iron conditions, and high NO_3^- concentrations (Jiang et al., 2018; Knapp et al., 2012; Kustka et al., 2003). NH_4^+ aerosols are unlikely to be abundant over regions of the Southern Ocean remote from islands and coastal Antarctica, particularly in winter when NH_4^+ aerosol concentrations have been shown to reach a minimum (Legrand et al., 1998; Xu et al., 2019). Moreover, the aerosols that are present over the open Southern Ocean will derive mainly from surface-ocean NH_3 efflux; once re-deposited, this NH_4^+ does not constitute a new input to surface waters (Altieri et al., 2021). Finally, since our sampling took place before the sea-ice reached its northernmost extent (Cavalieri & Parkinson, 2008), the dominant process would have been sea-ice formation rather than sea-ice melt, the latter an occasional source of NH_4^+ (Kattner et al., 2004; Zhou et al., 2014). In any case, we observed elevated NH_4^+ concentrations as far north as 46ºS, ~1700 km beyond the influence of sea-ice melt.

5.2 Seasonal cycling of NH_4^+ in the Southern Ocean mixed layer south of the SAF

The NH_4^+ concentration data collected over the 2018/19 annual cycle provide context for interpreting our winter 2017 dataset, allowing us to address our hypothesis that NH_4^+ production in late summer and autumn contributes to the elevated NH_4^+ concentrations measured in winter.

The very low NH_4^+ concentrations observed in early summer (Fig. 8a) are consistent with high rates of phytoplankton NH_4^+ assimilation during the spring and early-summer growing period (Mdutyana et al., 2020; Savoye et al., 2004; Daly et al., 2001). By late summer, the NH_4^+ concentrations increased (Fig. 8b) due to elevated heterotrophic activity (i.e., bacterial decomposition and zooplankton grazing) following the accumulation of algal biomass (Mengesha et al., 1998; Le Moigne et al., 2013), coupled with iron- and/or silicate-limitation of phytoplankton (Hiscock et al., 2003; Sosik & Olson, 2002) and enhanced grazing pressure (Becquevort et al., 2000). Mixed-layer NH_4^+ remained high between late summer and winter (Fig. 8b-c), likely due to sustained heterotrophic NH_4^+ production in excess of NH_4^+ removal. This notion is supported by estimates of the residence time of NH_4^+. We calculate that in summer, the in situ NH_4^+ pool would be depleted in 2 to 27 days (median of 5 days) without coincident NH_4^+ production. In addition, the net decline in NH_4^+ concentration of 0.31 ± 0.97 µM between late summer and winter requires an average NH_4^+ production rate of 52.8 ± 25.0 nM/day given the observed NH_4^+ assimilation rates. This estimate is remarkably similar to the only

769 measurements of NH_4^+ regeneration available for the Southern Ocean, measured near the
770 Antarctic Peninsula in summer (average of 55 nM day^{-1}; Goeyens et al., 1991).

771 By early spring, the NH_4^+ concentrations had declined (Fig. 8d), implicating increased
772 photosynthetic activity, and thus nutrient assimilation, following the alleviation of light-
773 limitation. We suggest that any NH_4^+ remaining in late winter would have been consumed in
774 early spring prior to significant NO_3^- drawdown because far less energy (i.e., light) is required
775 for its assimilation (Dortch, 1990). The high NH_4^+ concentrations subsequently observed in late
776 spring (mainly in the PFZ; Fig. 8e) can be explained by elevated heterotrophic activity in
777 response to high levels of regional phytoplankton growth driven by frontal upwelling of limiting
778 nutrients (Becquevort et al., 2000; Mayzaud et al., 2002).

779 From our six transects of surface NH_4^+ concentrations across the Southern Ocean, we propose a
780 seasonal cycle for mixed-layer NH_4^+ south of the SAF (Fig. 8f). Our proposal is consistent with
781 previous characterizations of the early summer-to-autumn evolution of Southern Ocean NH_4^+
782 concentrations (i.e., from below detection due to phytoplankton assimilation to elevated due to
783 net heterotrophy). However, it contradicts the hypothesis that NH_4^+ will subsequently decline due
784 to persistent but low rates of photosynthesis that yield insufficient biomass to support elevated
785 heterotrophy in autumn, thus driving a coincident decrease in photosynthetic and heterotrophic
786 activity (Koike et al., 1986; Serebrennikova & Fanning, 2004). Instead, our data evince a gradual
787 decline in mixed-layer NH_4^+ concentrations from late summer through winter. This decline can
788 be explained by heterotrophic NH_4^+ production outpacing NH_4^+ removal in late summer/autumn,
789 with NH_4^+ regeneration then decreasing during winter to lower rates than the combined rate of
790 NH_4^+ assimilation and oxidation. By late spring, NH_4^+ reaches concentrations similar to those
791 observed in early summer as the improved growing conditions (i.e., elevated light and iron
792 availability; Ellwood et al., 2008; Mtshali et al., 2019) allow phytoplankton to rapidly consume
793 any NH_4^+ remaining at the end of winter and subsequently produced in spring. An exception to
794 this scenario is elevated, localized NH_4^+ production near fronts, such as we observed in late spring
795 2019, which likely resulted from biological activity supported by frontal upwelling of silicate-
796 and iron-bearing Upper Circumpolar Deep Water (Prézelin et al., 2000).

797 ## 6. Summary and implications

798 Our study of the upper Southern Ocean, focused on the infrequently-sampled winter season,
799 provides new insights into the internal cycling of N in the mixed layer of a globally-important
800 region. We attribute the elevated NH_4^+ concentrations that persist in the winter mixed layer south
801 of the SAF to sustained heterotrophic NH_4^+ production in excess of NH_4^+ removal, driven by
802 temperature-, light-, and possibly iron-limitation of phytoplankton and nitrifiers. We further
803 suggest that heterotrophic bacteria are the main NH_4^+ producers in winter and that the
804 contribution of external sources to the Southern Ocean's mixed-layer NH_4^+ pool is negligible.
805 From observations of surface NH_4^+ concentrations made between December 2018 and November
806 2019, we deduce that the elevated mixed-layer NH_4^+ concentrations measured in winter cannot
807 be due solely to wintertime NH_4^+ production. Instead, we propose that NH_4^+ accumulates to its
808 highest concentrations in late summer following the peak phytoplankton growing season, after
809 which sustained heterotrophy throughout the autumn and winter prevents this NH_4^+ from being
810 fully depleted until the early spring, even though the rate of NH_4^+ removal must exceed that of

NH_4^+ production over this period. Measurements of heterotrophic NH_4^+ production rates are required to confirm the hypothesized seasonal cycle of NH_4^+ in the Southern Ocean mixed layer, and higher spatial resolution sampling of plankton community composition and N removal rates may help to explain local variability in NH_4^+ concentrations, particularly near the fronts.

The persistence of elevated NH_4^+ concentrations across the polar Southern Ocean between late summer and winter implies that the mixed layer is a biological source of CO_2 to the atmosphere for half the year, not only because NO_3^- drawdown is weak at this time (e.g., Gibson & Trull, 1999; Gray et al., 2018; Hauck et al., 2015; Mongwe et al., 2018; Shadwick et al., 2015), but also because the ambient conditions allow for NH_4^+ accumulation. There are additional implications of our observations. For example, NH_4^+ concentrations >1 μM (and at times >0.5 μM) have been reported to inhibit NO_3^- assimilation, including in the Southern Ocean (Cochlan, 1986; Goeyens et al., 1995; Philibert et al., 2015; Reay et al., 2001). Inhibition of NO_3^- assimilation due to the seasonal accumulation of NH_4^+ would constitute an inefficiency in the biological pump. However, we observed little evidence of this effect in winter 2017 – the southward decrease in ρNO_3^- was not stronger than that of ρNH_4^+ despite the latitudinal increase in NH_4^+ concentration, and we observed no relationship between NH_4^+ concentration and the proportion of NO_3^- to NO_3^-+NH_4^+ uptake (i.e., the f-ratio; Table S1).

The implications of NH_4^+ cycling extend beyond the upper ocean to the atmosphere, since ammonium aerosols that influence Earth's albedo (Tevlin & Murphy, 2019) are formed in the marine boundary layer from reactions of NH_3 gas with acidic species. In the remote Southern Ocean, marine NH_3 emissions, which are the largest natural contributors to NH_3 globally, are likely the dominant local source of NH_3 to the atmosphere (Paulot et al., 2015). Surface ocean NH_4^+ concentrations play a central role in determining the sign and magnitude of the air-sea NH_3 flux, along with wind speed, surface ocean temperature, and pH. Therefore, the biogeochemical pathways that underpin seasonal changes in surface ocean NH_4^+ concentrations represent an important control on the remote Southern Ocean air-sea NH_3 flux, with consequences for aerosol composition, cloud formation, and climate (Altieri et al., 2021).

Acknowledgements

We are grateful to Captain Knowledge Bengu and the crew of the R/V *SA Agulhas II*, and Chief Scientists Hermann Luyt, Marcello Vichi, and Thomas Ryan-Keogh. We thank Tahlia Henry for CTD operations and CTD and SDS data processing. We are grateful to the students from the Cape Peninsula University of Technology for help with sample collection and analysis of chl-a, and thank Raquel Flynn, Mishka Rawatlal, and Raymond Roman for assistance with nutrient analyses. We acknowledge the Flow Cytometry Core Facility at the University of Cape Town (UCT) and the efforts of Ian Newton at the Stable Light Isotope Laboratory (UCT). This work was supported by the South African Departments of Forestry, Fisheries, and Environment (formerly Environmental Affairs) and Science and Innovation (DSI), and the National Research Foundation (NRF) through the South African National Antarctic Program (SANAP; 110732 to K.E.A and 105539, 110735, and 129232 to S.E.F.), Equipment-related Travel and Training Grant (118615 to K.E.A.), Competitive Support for Rated Researchers Grant (111716 to K.E.A.), and Incentive Fund (115335 to S.E.F.). S.S., M.M., K.A.M.S., and J.M.B. acknowledge funding from the NRF through postgraduate scholarships (120105, 112380, 113193, and 108757). S.S. was partially supported by a UCT Vice-Chancellor Research Scholarship and M.M. by the UCT Harry Crossley Foundation Research Fellowship. S.E.F. and K.E.A. acknowledge the support of the UCT Vice-Chancellor Future Leaders 2030 programme. S.E.F. acknowledges an African Academy of Sciences/Royal Society FLAIR fellowship and K.E.A. acknowledges support from UCT through a University Research Council Launching Grant and a University Equipment Committee Grant. We further acknowledge the support of the DSI Biogeochemistry Research Infrastructure Platform (BIOGRIP).

7. References

Aarnos, H., Ylöstalo, P. and Vähätalo, A.V., (2012). Seasonal phototransformation of dissolved organic matter to ammonium, dissolved inorganic carbon, and labile substrates supporting bacterial biomass across the Baltic Sea. *Journal of Geophysical Research: Biogeosciences*, 117(G1).

Alldredge, A.L. and Gotschalk, C., (1988). In situ settling behavior of marine snow 1. *Limnology and Oceanography*, 33(3), pp.339-351.

Altabet, M.A., (1988). Variations in nitrogen isotopic composition between sinking and suspended particles: Implications for nitrogen cycling and particle transformation in the open ocean. *Deep Sea Research Part A. Oceanographic Research Papers*, 35(4), pp.535-554.

Altieri, K.E., Spence, K.A.M., and Smith, S. (2021). Air-Sea Ammonia Fluxes Calculated from High-Resolution Summertime Observations Across the Atlantic Southern Ocean. *Geophysical Research Letters*.

Amin, S.A., Moffett, J.W., Martens-Habbena, W., Jacquot, J.E., Han, Y., Devol, A., Ingalls, A.E., Stahl, D.A. and Armbrust, E.V., (2013). Copper requirements of the ammonia-oxidizing archaeon Nitrosopumilus maritimus SCM1 and implications for nitrification in the marine environment. *Limnology and Oceanography*, 58(6), pp.2037-2045.

Armstrong, R.A., (1999). An optimization-based model of iron-light-ammonium colimitation of nitrate uptake and phytoplankton growth. *Limnology and Oceanography*, 44(6), pp.1436-1446.

Arrigo, K. R., van Dijken, G. L., and Bushinsky, S. (2008). Primary production in the Southern Ocean, 1997–2006. *Journal of Geophysical Research*, *113*(C8), C08004.

Arteaga, L.A., Pahlow, M., Bushinsky, S.M. and Sarmiento, J.L., (2019). Nutrient controls on export production in the Southern Ocean. *Global Biogeochemical Cycles*, 33(8), pp.942-956.

Atkinson, A., Ward, P., Hunt, B.P.V., Pakhomov, E.A. and Hosie, G.W., (2012). An overview of Southern Ocean zooplankton data: abundance, biomass, feeding and functional relationships. *CCLAMR Science*, 19, pp.171-218.

Baer, S.E., Connelly, T.L., Sipler, R.E., Yager, P.L. and Bronk, D.A., (2014). Effect of temperature on rates of ammonium uptake and nitrification in the western coastal Arctic during winter, spring, and summer. *Global Biogeochemical Cycles*, *28*(12), pp.1455-1466.

Bagwell, J.E., (2009). Transcriptional Response of Nitrogen Uptake and Assimilation in Marine Diatoms; Thalassiosira Pseudonana and Thalassiosira Weissflogii (Doctoral dissertation, University of North Carolina Wilmington).

Baird, M.E., Emsley, S.M. and Mcglade, J.M., (2001). Modelling the interacting effects of nutrient uptake, light capture and temperature on phytoplankton growth. *Journal of Plankton Research*, *23*(8), pp.829-840.

Bakker, D. C. E., Pfeil, B., Landa, C. S., Metzl, N., O'Brien, K. M., Olsen, A., et al. (2016). A multi-decade record of high-quality FCO2 data in version 3 of the Surface Ocean CO2 Atlas (SOCAT). *Earth System Science Data*, 8, 383–413.

Bathmann, U.V., Scharek, R., Klaas, C., Dubischar, C.D. and Smetacek, V., (1997). Spring development of phytoplankton biomass and composition in major water masses of the Atlantic sector of the Southern Ocean. Deep Sea Research Part II: Topical Studies in Oceanography, 44(1-2), pp.51-67.

Becquevort, S., Menon, P., and Lancelot, C. (2000). Differences of the protozoan biomass and grazing during spring and summer in the Indian sector of the Southern Ocean. *Polar Biology*, *23*(5), 309–320.

Belkin, I. M., and Gordon, A. L. (1996). Southern Ocean fronts from the Greenwich meridian to Tasmania. *Journal of Geophysical Research C: Oceans*, 101(C2), 3675–3696.

Bendschneider, K. and Robinson, R.J., (1952). A new spectrophotometric method for the determination of nitrite in sea water.

Bianchi, M., Feliatra, F., Tréguer, P., Vincendeau, M.A. and Morvan, J., (1997). Nitrification rates, ammonium and nitrate distribution in upper layers of the water column and in sediments of the Indian sector of the Southern Ocean. *Deep Sea Research Part II: Topical Studies in Oceanography*, *44*(5), pp.1017-1032.

Billen, G., (1984). Heterotrophic utilization and regeneration of nitrogen. In *Heterotrophic activity in the sea*. NATO Conference Series (IV Marine Sciences), vol 15. Springer, Boston, MA.

Bouwman, A. F., Lee, D. S., Asman, W. A. H., Dentener, F. J., Van Der Hoek, K. W., and Olivier, J. G. J. (1997). A global high-resolution emission inventory for ammonia. *Global Biogeochemical Cycles*, *11*(4), 561–587.

Boyd, P.W., Crossley, A.C., DiTullio, G.R., Griffiths, F.B., Hutchins, D.A., Queguiner, B., Sedwick, P.N. and Trull, T.W., (2001). Control of phytoplankton growth by iron supply and irradiance in the subantarctic Southern Ocean: Experimental results from the SAZ Project. *Journal of Geophysical Research: Oceans*, *106*(C12), pp.31573-31583.

Boyd, P. W., Rynearson, T. A., Armstrong, E. A., Fu, F., Hayashi, K., Hu, Z., Hutchins, D. A., Kudela, R. M., Litchman, E., Mulholland, M. R., Passow, U., Strzepek, R. F., Whittaker, K. A., Yu, E., and Thomas, M. K. (2013). Marine Phytoplankton Temperature versus Growth Responses from Polar to Tropical Waters - Outcome of a Scientific Community-Wide Study. *PLoS ONE*, *8*(5), 1–17.

Bracher, A. U., Kroon, B. M. A., and Lucas, M. I. (1999). Primary production, physiological state and composition of phytoplankton in the Atlantic sector of the Southern Ocean. *Marine Ecology Progress Series*, *190*, 1–16.

Brightman, R.I. and Smith Jr, W.O., (1989). Photosynthesis-irradiance relationships of Antarctic phytoplankton during austral winter. *Marine Ecology Progress Series*, pp.143-151.

Broecker, W.S. and Peng, T.H., (1992). Interhemispheric transport of carbon dioxide by ocean circulation. *Nature*, 356(6370), pp.587-589.

Brzezinski, M. A. (1988). Vertical distribution of ammonium in stratified oligotrophic waters. *Limnol. Oceanogr.* 33(5), 1176–1182.

Buongiorno Nardelli, B., Guinehut, S., Verbrugge, N., Cotroneo, Y., Zambianchi, E. and Iudicone, D., (2017). Southern Ocean mixed-layer seasonal and interannual variations from combined satellite and in situ data. *Journal of Geophysical Research: Oceans*, *122*(12), pp.10042-10060.

Campitelli E. (2019). metR: Tools for Easier Analysis of Meteorological Fields. R package version 0.5.0. https://CRAN.R-project.org/package=metR

Capone, D.G., Bronk, D.A., Mulholland, M.R. and Carpenter, E.J. eds., (2008). *Nitrogen in the marine environment*. Elsevier.

Carvalho, F., Kohut, J., Oliver, M.J. and Schofield, O., (2017). Defining the ecologically relevant mixed-layer depth for Antarctica's coastal seas. *Geophysical Research Letters*, *44*(1), pp.338-345.

Casey, J.R., Lomas, M.W., Michelou, V.K., Dyhrman, S.T., Orchard, E.D., Ammerman, J.W. and Sylvan, J.B., (2009). Phytoplankton taxon-specific orthophosphate (Pi) and ATP utilization in the western subtropical North Atlantic. *Aquatic microbial ecology*, 58(1), pp.31-44.

Cavagna, A.J., Fripiat, F., Elskens, M., Mangion, P., Chirurgien, L., Closset, I., Lasbleiz, M., Florez-Leiva, L., Cardinal, D., Leblanc, K., and Fernandez, C., (2015). Production regime and associated N cycling in the vicinity of Kerguelen Island, Southern Ocean. *Biogeosciences*, 12(21), pp.6515-6528.

Cavalieri, D.J. and Parkinson, C.L., (2008). Antarctic sea ice variability and trends, 1979–2006. *Journal of Geophysical Research: Oceans*, 113(C7).

Cavender-Bares, K.K., Mann, E.L., Chisholm, S.W., Ondrusek, M.E. and Bidigare, R.R., (1999). Differential response of equatorial Pacific phytoplankton to iron fertilization. *Limnology and Oceanography*, 44(2), pp.237-246.

Checkley Jr, D.M. and Miller, C.A., (1989). Nitrogen isotope fractionation by oceanic zooplankton. *Deep Sea Research Part A. Oceanographic Research Papers*, 36(10), pp.1449-1456.

945 Chisholm, S. W. (1992). Phytoplankton Size. In *Primary Productivity and Biogeochemical Cycles in the Sea* (pp. 213–
946 237). Springer US.

947 Church, M.J., DeLong, E.F., Ducklow, H.W., Karner, M.B., Preston, C.M. and Karl, D.M., (2003). Abundance and
948 distribution of planktonic Archaea and Bacteria in the waters west of the Antarctic Peninsula. *Limnology and*
949 *Oceanography*, *48*(5), pp.1893-1902.

950 Coale, K. H., Gordon, R. M., and Wang, X. (2005). The distribution and behaviour of dissolved and particulate iron and
951 zinc in the Ross Sea and Antarctic circumpolar current along 170°W. *Deep-Sea Research Part I: Oceanographic*
952 *Research Papers*, *52*(2), 295–318.

953 Cochlan, W.P., (1986). Seasonal study of uptake and regeneration of nitrogen on the Scotian Shelf. Continental Shelf
954 Research, 5(5), pp.555-577.

955 Cochlan, W.P., (2008). Nitrogen uptake in the Southern Ocean. *Nitrogen in the Marine Environment*, edited by: Capone,
956 DG, Bronk, DA, Mulholland, MR, and Carpenter, EJ, 2nd Edition, Academic Press, Elsevier, pp.569-596.

957 Cochlan, W.P., Bronk, D.A. and Coale, K.H., (2002). Trace metals and nitrogenous nutrition of Antarctic phytoplankton:
958 experimental observations in the Ross Sea. *Deep Sea Research Part II: Topical Studies in Oceanography*, 49(16),
959 pp.3365-3390.

960 Coello-Camba, A. and Agustí, S., (2017). Thermal thresholds of phytoplankton growth in polar waters and their
961 consequences for a warming polar ocean. *Frontiers in Marine Science*, *4*, p.168.

962 Cota, G.F., Smith, W.O., Nelson, D.M., Muench, R.D. and Gordon, L.I., (1992). Nutrient and biogenic particulate
963 distributions, primary productivity and nitrogen uptake in the Weddell-Scotia Sea marginal ice zone during winter.
964 *Journal of Marine Research*, *50*(1), pp.155-181

965 Daly, K. L., Smith, W. O., Johnson, G. C., DiTullio, G. R., Jones, D. R., Mordy, C. W., Feely, R. A., Hansell, D. A., and
966 Zhang, J.-Z. (2001). Hydrography, nutrients, and carbon pools in the Pacific sector of the Southern Ocean: Implications
967 for carbon flux. *Journal of Geophysical Research: Oceans*, *106*(C4), 7107–7124.

968 Deary, A. (2020). A high-resolution study of the early- to late summer progression in primary production and carbon
969 export potential in the Atlantic Southern Ocean. (Honours thesis, University of Cape Town).

970 del Giorgio, P.A. and Cole, J.J., (1998). Bacterial growth efficiency in natural aquatic systems. *Annual Review of Ecology*
971 *and Systematics*, 29(1), pp.503-541.

972 Dennett, M. R., Mathot, S., Caron, D. A., Smith, W. O., and Lonsdale, D. J. (2001). Abundance and distribution of
973 phototrophic and heterotrophic nano- and microplankton in the southern Ross Sea. *Deep-Sea Research Part II: Topical*
974 *Studies in Oceanography*, *48*(19–20), 4019–4037.

975 Deppeler, S.L. and Davidson, A.T., (2017). Southern Ocean phytoplankton in a changing climate. *Frontiers in Marine*
976 *Science*, 4, p.40.

977 Detmer, A.E. and Bathmann, U.V., (1997). Distribution patterns of autotrophic pico-and nanoplankton and their relative
978 contribution to algal biomass during spring in the Atlantic sector of the Southern Ocean. *Deep Sea Research Part II:*
979 *Topical Studies in Oceanography*, *44*(1-2), pp.299-320.

980 DiFiore, P. J., Sigman, D. M., Trull, T. W., Lourey, M. J., Karsh, K., Cane, G., and Ho, R. (2006). Nitrogen isotope
981 constraints on subantarctic biogeochemistry. *Journal of Geophysical Research: Oceans*, *111*(8).

982 Dixon, G.K. and Syrett, P.J., (1988). The growth of dinoflagellates in laboratory cultures. *New phytologist*, *109*(3),
983 pp.297-302.

984 Doney, S.C., Mahowald, N., Lima, I., Feely, R.A., Mackenzie, F.T., Lamarque, J.F. and Rasch, P.J., (2007). Impact of
985 anthropogenic atmospheric nitrogen and sulfur deposition on ocean acidification and the inorganic carbon
986 system. *Proceedings of the National Academy of Sciences*, *104*(37), pp.14580-14585.

987 Dong, S., Sprintall, J., Gille, S.T. and Talley, L., (2008). Southern Ocean mixed-layer depth from Argo float profiles.
988 *Journal of Geophysical Research: Oceans*, *113*(C6).

989 Dortch, Q. (1990). The interaction between ammonium and nitrate uptake in phytoplankton. *Marine Ecology Progress*
990 *Series*, *61*(1), 183–201.

991 Dugdale, R. C., and Goering, J. J. (1967). Uptake of new and regenerated forms of nitrogen in primary productivity.
992 *Limnology and Oceanography*, *12*(2), 196–206.

993 Dugdale, R.C. and Wilkerson, F.P., (1986). The use of 15N to measure nitrogen uptake in eutrophic oceans; experimental
994 considerations 1, 2. *Limnology and Oceanography*, *31*(4), pp.673-689.

995 Ellwood, M.J., Boyd, P.W. and Sutton, P., (2008). Winter-time dissolved iron and nutrient distributions in the
996 Subantarctic Zone from 40–52S; 155–160E. *Geophysical Research Letters*, 35(11).

997 El-Sayed, S., (1984). Productivity of the Antarctic waters—a reappraisal. In *Marine phytoplankton and productivity* (pp.
998 19-34). Springer, Berlin, Heidelberg.

999 Eppley, R.W. and Peterson, B.J., (1979). Particulate organic matter flux and planktonic new production in the deep
1000 ocean. *Nature*, *282*(5740), pp.677-680.

Fan, C., Glibert, P.M., and Burkholder, J.M., (2003). Characterization of the affinity for nitrogen, uptake kinetics, and environmental relationships for Prorocentrum minimum in natural blooms and laboratory cultures. *Harmful Algae*, *2*(4), pp.283-299.

Fawcett, S. E., and Ward, B. B. (2011). Phytoplankton succession and nitrogen utilization during the development of an upwelling bloom. *Marine Ecology Progress Series*, 428, 13–31.

Fawcett, S.E., Lomas, M.W., Casey, J.R., Ward, B.B. and Sigman, D.M., (2011). Assimilation of upwelled nitrate by small eukaryotes in the Sargasso Sea. *Nature Geoscience*, 4(10), pp.717-722.

Fawcett, S.E., Lomas, M.W., Ward, B.B. and Sigman, D.M., (2014). The counterintuitive effect of summer-to-fall mixed layer deepening on eukaryotic new production in the Sargasso Sea. *Global biogeochemical cycles*, 28(2), pp.86-102.

Fiala, M. and Oriol, L., (1990). Light-temperature interactions on the growth of Antarctic diatoms. *Polar Biology*, *10*(8), pp.629-636.

Fiala, M., Semeneh, M. and Oriol, L., (1998). Size-fractionated phytoplankton biomass and species composition in the Indian sector of the Southern Ocean during austral summer. *Journal of Marine Systems*, *17*(1-4), pp.179-194.

Finkel, Z.V., Irwin, A.J. and Schofield, O., (2004). Resource limitation alters the 3/4 size scaling of metabolic rates in phytoplankton. *Marine Ecology Progress Series*, *273*, pp.269-279.

Finley A., Banerjee S., and Hjelle Ø. (2017). MBA: Multilevel B-Spline Approximation. package version 0.0-9. https://CRAN.R-project.org/package=MBA

Forsythe, W.C., Rykiel Jr, E.J., Stahl, R.S., Wu, H.I. and Schoolfield, R.M., (1995). A model comparison for daylength as a function of latitude and day of year. *Ecological Modelling*, 80(1), pp.87-95.

Flynn, R.F., Burger, J.M., Pillay, K. and Fawcett, S.E., (2018). Wintertime rates of net primary production and nitrate and ammonium uptake in the southern Benguela upwelling system. *African Journal of Marine Science*, 40(3), pp.253-266.

Franck, V.M., Smith, G.J., Bruland, K.W. and Brzezinski, M.A., (2005). Comparison of size-dependent carbon, nitrate, and silicic acid uptake rates in high-and low-iron waters. *Limnology and Oceanography*, 50(3), pp.825-838.

Francois, R., Altabet, M.A. and Burckle, L.H., (1992). Glacial to interglacial changes in surface nitrate utilization in the Indian sector of the Southern Ocean as recorded by sediment δ15N. *Paleoceanography*, *7*(5), pp.589-606.

Fransson, A., Chierici, M., Anderson, L. and David, R., (2004). Transformation of carbon and oxygen in the surface layer of the eastern Atlantic sector of the Southern Ocean. *Deep Sea Research Part II: Topical Studies in Oceanography*, *51*(22-24), pp.2757-2772.

Frigstad, H., Andersen, T., Hessen, D.O., Naustvoll, L.J., Johnsen, T.M. and Bellerby, R.G., (2011). Seasonal variation in marine C: N: P stoichiometry: can the composition of seston explain stable Redfield ratios?. *Biogeosciences*, 8(10), pp.2917-2933.

Fripiat, F., Elskens, M., Trull, T.W., Blain, S., Cavagna, A.J., Fernandez, C., Fonseca-Batista, D., Planchon, F., Raimbault, P., Roukaerts, A. and Dehairs, F., (2015). Significant mixed layer nitrification in a natural iron-fertilized bloom of the Southern Ocean. *Global Biogeochemical Cycles*, 29(11), pp.1929-1943.

Fripiat, F., Martínez-García, A., Fawcett, S.E., Kemeny, P.C., Studer, A.S., Smart, S.M., Rubach, F., Oleynik, S., Sigman, D.M. and Haug, G.H., (2019). The isotope effect of nitrate assimilation in the Antarctic Zone: Improved estimates and paleoceanographic implications. *Geochimica et Cosmochimica Acta*, 247, pp.261-279.

Fripiat, F., Martínez-García, A., Marconi, D., Fawcett, S.E., Kopf, S., Luu, V., Rafter, P., Zhang, R., Sigman, D., and Haug, G, (2021). Nitrogen isotopic constraints on nutrient transport to the upper ocean. *Nature Geoscience.*

Frölicher, T.L., Sarmiento, J.L., Paynter, D.J., Dunne, J.P., Krasting, J.P., and Winton, M., (2015). Dominance of the Southern Ocean in anthropogenic carbon and heat uptake in CMIP5 models. *Journal of Climate*, 28(2), pp.862-886.

Froneman, P.W., Ansorge, I.J., Pakhomov, E.A. and Lutjeharms, J.R.E., (1999). Plankton community structure in the physical environment surrounding the Prince Edward Islands (Southern Ocean). *Polar Biology*, *22*(3), pp.145-155.

Fujiki, T. and Taguchi, S., (2002). Variability in chlorophyll a specific absorption coefficient in marine phytoplankton as a function of cell size and irradiance. *Journal of Plankton Research*, *24*(9), pp.859-874.

Gao, Y., Kaufman, Y. J., Tanré, D., Kolber, D., and Falkowski, P. G. (2001). Seasonal distributions of aeolian iron fluxes to the global ocean. *Geophysical Research Letters*, *28*(1), pp.29–32.

Gasol, J.M. and del Giorgio, P.A., (2000). Using flow cytometry for counting natural planktonic bacteria and understanding the structure of planktonic bacterial communities. *Scientia Marina*, 64(2), pp.197-224.

Gibson, J.A. and Trull, T.W., (1999). Annual cycle of fCO2 under sea-ice and in open water in Prydz Bay, East Antarctica. *Marine Chemistry*, 66(3-4), pp.187-200.

Glibert, P.M., (1982). Regional studies of daily, seasonal and size fraction variability in ammonium remineralization. *Marine Biology*, 70(2), pp.209-222.

Goericke, R., (1998). Response of phytoplankton community structure and taxon-specific growth rates to seasonally varying physical forcing in the Sargasso Sea off Bermuda. *Limnology and Oceanography*, *43*(5), pp.921-935.

Goeyens, L., Tréguer, P., Lancelot, C., Mathot, S., Becquevort, S., Morvan, J., Dehairs, F. and Baeyens, W., (1991). Ammonium regeneration in the Scotia-Weddell Confluence area during spring 1988. *Marine Ecology Progress Series*, pp.241-252.

Goeyens, L., Tréguer, P., Baumann, M. E. M., Baeyens, W., and Dehairs, F. (1995). The leading role of ammonium in the nitrogen uptake regime of Southern Ocean marginal ice zones. *Journal of Marine Systems*, *6*(4), pp.345–361.

Granger, J., Sigman, D.M., Needoba, J.A. and Harrison, P.J., (2004). Coupled nitrogen and oxygen isotope fractionation of nitrate during assimilation by cultures of marine phytoplankton. *Limnology and Oceanography,* 49(5), pp.1763-1773.

Granger, J., Sigman, D.M., Rohde, M.M., Maldonado, M.T. and Tortell, P.D., (2010). N and O isotope effects during nitrate assimilation by unicellular prokaryotic and eukaryotic plankton cultures. *Geochimica et Cosmochimica Acta*, 74(3), pp.1030-1040.

Gray, A.R., Johnson, K.S., Bushinsky, S.M., Riser, S.C., Russell, J.L., Talley, L.D., Wanninkhof, R., Williams, N.L. and Sarmiento, J.L., (2018). Autonomous biogeochemical floats detect significant carbon dioxide outgassing in the high-latitude Southern Ocean. *Geophysical Research Letters*, 45(17), pp.9049-9057.

Greene, R.M., Geider, R.J. and Falkowski, P.G., (1991). Effect of iron limitation on photosynthesis in a marine diatom. *Limnology and Oceanography*, *36*(8), pp.1772-1782.

Harrison, W.G., (1976). Nitrate metabolism of the red tide dinoflagellate Gonyaulax polyedra Stein. *Journal of Experimental Marine Biology and Ecology*, *21*(3), pp.199-209.

Hasle, R.G., (1978). The inverted microscope method. *Phytoplankton manual*, pp.88-96.

Hauck, J., Völker, C., Wolf-Gladrow, D.A., Laufkötter, C., Vogt, M., Aumont, O., Bopp, L., Buitenhuis, E.T., Doney, S.C., Dunne, J. and Gruber, N., (2015). On the Southern Ocean CO2 uptake and the role of the biological carbon pump in the 21st century. *Global Biogeochemical Cycles*, 29(9), pp.1451-1470.

Henley, S.F., Tuerena, R.E., Annett, A.L., Fallick, A.E., Meredith, M.P., Venables, H.J., Clarke, A. and Ganeshram, R.S., (2017). Macronutrient supply, uptake and recycling in the coastal ocean of the west Antarctic Peninsula. *Deep Sea Research Part II: Topical Studies in Oceanography*, 139, pp.58-76.

Henley, S.F., Cavan, E.L., Fawcett, S.E., Kerr, R., Monteiro, T., Sherrell, R.M., Bowie, A.R., Boyd, P.W., Barnes, D.K., Schloss, I.R., Marshall, T., Flynn, R., and Smith, S., (2020). Changing biogeochemistry of the Southern Ocean and its ecosystem implications. *Frontiers in Marine Science*, 7, p.581.

Hense, I., Bathmann, U.V. and Timmermann, R., (2000). Plankton dynamics in frontal systems of the Southern Ocean. *Journal of Marine Systems*, *27*(1-3), pp.235-252.

Herbert, R.A., (1999). Nitrogen cycling in coastal marine ecosystems. *FEMS microbiology reviews*, *23*(5), pp.563-590.

Hewes, C.D., Holm-Hansen, O. and Sakshaug, E., (1985). Alternate carbon pathways at lower trophic levels in the Antarctic food web. *Antarctic nutrient cycles and food webs*. pp. 277-28.

Hewes, C.D., Sakshaug, E., Reid, F.M., and Holm-Hansen, O., (1990). Microbial autotrophic and heterotrophic eucaryotes in Antarctic waters: relationships between biomass and chlorophyll, adenosine triphosphate and particulate organic carbon. *Marine Ecology Progress Series*, pp.27-35.

Hiscock, M.R., Marra, J., Smith Jr, W.O., Goericke, R., Measures, C., Vink, S., Olson, R.J., Sosik, H.M. and Barber, R.T., (2003). Primary productivity and its regulation in the Pacific Sector of the Southern Ocean. *Deep Sea Research Part II: Topical Studies in Oceanography*, 50(3-4), pp.533-558.

Holm-Hansen, O., Mitchell, B.G., Hewes, C.D. and Karl, D.M., (1989). Phytoplankton blooms in the vicinity of Palmer Station, Antarctica. *Polar Biology*, 10(1), pp.49-57.

Holmes, R.M., Aminot, A., Kérouel, R., Hooker, B.A. and Peterson, B.J., (1999). A simple and precise method for measuring ammonium in marine and freshwater ecosystems. *Canadian Journal of Fisheries and Aquatic Sciences*, *56*(10), pp.1801-1808.

Holzer, M., Primeau, F.W., DeVries, T. and Matear, R., (2014). The Southern Ocean silicon trap: Data-constrained estimates of regenerated silicic acid, trapping efficiencies, and global transport paths. *Journal of Geophysical Research: Oceans*, *119*(1), pp.313-331.

Honjo, S., Francois, R., Manganini, S., Dymond, J. and Collier, R., (2000). Particle fluxes to the interior of the Southern Ocean in the Western Pacific sector along 170 W. *Deep Sea Research Part II: Topical Studies in Oceanography*, *47*(15-16), pp.3521-3548.

Hooper, A.B. and Terry, K.R., (1974). Photoinactivation of ammonia oxidation in Nitrosomonas. *Journal of Bacteriology*, 119(3), pp.899-906.

Horak, R.E., Qin, W., Schauer, A.J., Armbrust, E.V., Ingalls, A.E., Moffett, J.W., Stahl, D.A. and Devol, A.H., (2013). Ammonia oxidation kinetics and temperature sensitivity of a natural marine community dominated by Archaea. *The ISME journal*, 7(10), pp.2023-2033.

Horrigan, S. G., & Springer, A. L. (1990). Oceanic and estuarine ammonium oxidation: Effects of light. *Limnology and Oceanography*, *35*(2), pp.479–482.

Huang, K., Feng, Q., Zhang, Y., Ou, L., Cen, J., Lu, S. and Qi, Y., (2020). Comparative uptake and assimilation of nitrate, ammonium, and urea by dinoflagellate Karenia mikimotoi and diatom Skeletonema costatum sl in the coastal waters of the East China Sea. *Marine Pollution Bulletin*, *155*, p.111200.

Hudson, R.J. and Morel, F.M., (1993). Trace metal transport by marine microorganisms: implications of metal coordination kinetics. *Deep Sea Research Part I: Oceanographic Research Papers*, *40*(1), pp.129-150.

Hutchins, D.A., Sedwick, P.N., DiTullio, G.R., Boyd, P.W., Queguiner, B., Griffiths, F.B. and Crossley, C., (2001). Control of phytoplankton growth by iron and silicic acid availability in the subantarctic Southern Ocean: Experimental results from the SAZ Project. *Journal of Geophysical Research: Oceans*, *106*(C12), pp.31559-31572.

Iida, T. and Odate, T., (2014). Seasonal variability of phytoplankton biomass and composition in the major water masses of the Indian Ocean sector of the Southern Ocean. *Polar Science*, *8*(3), pp.283-297.

Ishikawa, A., Wright, S.W., van den Enden, R., Davidson, A.T. and Marchant, H.J., (2002). Abundance, size structure and community composition of phytoplankton in the Southern Ocean in the austral summer 1999/2000. *Polar Biosciences*. 15, pp.11-26.

Jacobson, D. M., and Anderson, D. M. (1996). Widespread phagocytosis of ciliates and other protists by marine mixotrophic and heterotrophic thecate dinoflagellates. *Journal of Phycology*, *32*(2), 279–285.

Janssen, D.J., Sieber, M., Ellwood, M.J., Conway, T.M., Barrett, P.M., Chen, X., de Souza, G.F., Hassler, C.S. and Jaccard, S.L., (2020). Trace metal and nutrient dynamics across broad biogeochemical gradients in the Indian and Pacific sectors of the Southern Ocean. *Marine chemistry*, *221*, p.103773.

Jeong, H.J. and Latz, M.I., (1994). Growth and grazing rates of the heterotrophic dinoflagellates Protoperidinium spp. on red tide dinoflagellates. *Marine Ecology-Progress Series*, *106*, pp.173-173.

Jiang, H.B., Fu, F.X., Rivero-Calle, S., Levine, N.M., Sañudo-Wilhelmy, S.A., Qu, P.P., Wang, X.W., Pinedo-Gonzalez, P., Zhu, Z. and Hutchins, D.A., (2018). Ocean warming alleviates iron limitation of marine nitrogen fixation. *Nature Climate Change*, *8*(8), pp.709-712.

Johnson, K.S., Plant, J.N., Dunne, J.P., Talley, L.D. and Sarmiento, J.L., (2017). Annual nitrate drawdown observed by SOCCOM profiling floats and the relationship to annual net community production. *Journal of Geophysical Research: Oceans*, *122*(8), pp.6668-6683.

Jones, R.D., Morita, R.Y., Koops, H.P. and Watson, S.W., (1988). A new marine ammonium-oxidizing bacterium, Nitrosomonas cryotolerans sp. nov. *Canadian journal of microbiology*, *34*(10), pp.1122-1128.

Joubert, W. R., Thomalla, S. J., Waldron, H. N., Lucas, M. I., Boye, M., Le Moigne, F. A. C., Planchon, F., and Speich, S. (2011). Nitrogen uptake by phytoplankton in the Atlantic sector of the Southern Ocean during late austral summer. *Biogeosciences*, *8*(10), pp.2947–2959.

Kassambara A. (2019). ggpubr: 'ggplot2' Based Publication Ready Plots. R package version 0.2.4. https://CRAN.R-project.org/package=ggpubr

Kattner, G., Thomas, D.N., Haas, C., Kennedy, H. and Dieckmann, G.S., (2004). Surface ice and gap layers in Antarctic sea ice: highly productive habitats. *Marine Ecology Progress Series*, 277, pp.1-12.

Kemeny, P.C., Kast, E.R., Hain, M.P., Fawcett, S.E., Fripiat, F., Studer, A.S., Martínez-García, A., Haug, G.H. and Sigman, D.M., (2018). A seasonal model of nitrogen isotopes in the ice age Antarctic Zone: Support for weakening of the Southern Ocean upper overturning cell. *Paleoceanography and Paleoclimatology*, 33(12), pp.1453-1471.

Kirchman, D. L. (1994). The Uptake of Inorganic Nutrients by Heterotrophic Bacteria. *Microbial Ecology* 28(2), pp.255–71.

Kitzinger, K., Padilla, C.C., Marchant, H.K., Hach, P.F., Herbold, C.W., Kidane, A.T., Könneke, M., Littmann, S., Mooshammer, M., Niggemann, J. and Petrov, S., (2019). Cyanate and urea are substrates for nitrification by Thaumarchaeota in the marine environment. Nature microbiology, 4(2), pp.234-243.

Klawonn, I., Bonaglia, S., Whitehouse, M.J., Littmann, S., Tienken, D., Kuypers, M.M., Brüchert, V. and Ploug, H., (2019). Untangling hidden nutrient dynamics: rapid ammonium cycling and single-cell ammonium assimilation in marine plankton communities. *The ISME journa*l, 13(8), pp.1960-1974.

Knapp, A.N., Dekaezemacker, J., Bonnet, S., Sohm, J.A. and Capone, D.G., (2012). Sensitivity of Trichodesmium erythraeum and Crocosphaera watsonii abundance and N2 fixation rates to varying NO3− and PO43− concentrations in batch cultures. *Aquatic microbial ecology*, 66(3), pp.223-236.

Kobayashi, F. and Takahashi, K., (2002). Distribution of diatoms along the equatorial transect in the western and central Pacific during the 1999 La Niña conditions. *Deep Sea Research Part II: Topical Studies in Oceanography*, *49*(13-14), pp.2801-2821.

Koike, I., Holm-Hansen, O., and Biggs, D. C. (1986). Phytoplankton With Special Reference To Ammonium Cycling. *Marine Ecology*, *30*, pp.105–116.

Kopczyńska, E. E., Savoye, N., Dehairs, F., Cardinal, D., and Elskens, M. (2007). Spring phytoplankton assemblages in the Southern Ocean between Australia and Antarctica. *Polar Biology*, *31*(1), pp.77–88.

Kottmeier, S.T. and Sullivan, C.W., (1987). Late winter primary production and bacterial production in sea ice and seawater west of the Antarctic Peninsula. *Mar Ecol Prog Ser*, *36*, pp.287-298.

Krell, A., Schnack-Schiel, S.B., Thomas, D.N., Kattner, G., Zipan, W. and Dieckmann, G.S., (2005). Phytoplankton dynamics in relation to hydrography, nutrients and zooplankton at the onset of sea ice formation in the eastern Weddell Sea (Antarctica). *Polar Biology*, 28(9), pp.700-713.

Kristiansen, S. and Farbrot, T., (1991). Nitrogen uptake rates in phytoplankton and ice algae in the Barents Sea. *Polar research*, 10(1), pp.187-192.

Kustka, A.B., Sañudo-Wilhelmy, S.A., Carpenter, E.J., Capone, D., Burns, J. and Sunda, W.G., (2003). Iron requirements for dinitrogen-and ammonium-supported growth in cultures of Trichodesmium (IMS 101): Comparison with nitrogen fixation rates and iron: Carbon ratios of field populations. *Limnology and Oceanography*, 48(5), pp.1869-1884.

La Roche, J. (1983). Ammonium regeneration: its contribution to phytoplankton nitrogen requirements in a eutrophic environment. *Marine Biology*, *75*(2–3), pp.231–240.

Landry, M.R., Selph, K.E., Brown, S.L., Abbott, M.R., Measures, C.I., Vink, S., Allen, C.B., Calbet, A., Christensen, S. and Nolla, H., (2002). Seasonal dynamics of phytoplankton in the Antarctic Polar Front region at 170° W. *Deep Sea Research Part II: Topical Studies in Oceanography*, *49*(9-10), pp.1843-1865.

Laubscher, R.K., Perissinotto, R. and McQuaid, C.D., (1993). Phytoplankton production and biomass at frontal zones in the Atlantic sector of the Southern Ocean. *Polar biology*, *13*(7), pp.471-481.

Lauderdale, J.M., Garabato, A.C.N., Oliver, K.I., Follows, M.J. and Williams, R.G., (2013). Wind-driven changes in Southern Ocean residual circulation, ocean carbon reservoirs and atmospheric CO 2. *Climate dynamics*, *41*(7-8), pp.2145-2164.

Lee, S.H., Joo, H.M., Liu, Z., Chen, J. and He, J., (2012). Phytoplankton productivity in newly opened waters of the Western Arctic Ocean. *Deep Sea Research Part II: Topical Studies in Oceanography*, *81*, pp.18-27.

Lee, S.H., Yun, M.S., Kim, B.K., Joo, H., Kang, S.H., Kang, C.K. and Whitledge, T.E., (2013). Contribution of small phytoplankton to total primary production in the Chukchi Sea. *Continental Shelf Research*, *68*, pp.43-50.

Legrand, M., Ducroz, F., Wagenbach, D., Mulvaney, R. and Hall, J., (1998). Ammonium in coastal Antarctic aerosol and snow: Role of polar ocean and penguin emissions. *Journal of Geophysical Research: Atmospheres*, 103(D9), pp.11043-11056.

Lehette, P., Tovar-Sánchez, A., Duarte, C.M. and Hernández-León, S., (2012). Krill excretion and its effect on primary production. *Marine Ecology Progress Series*, *459*, pp.29-38.

Le Moigne, F. A., Boye, M., Masson, A., Corvaisier, R., Grossteffan, E., Gueneugues, A., Pondaven, P., Le Moigne, F. A. C., Boye, M., Corvaisier, R., Guéneugues, A., & Pondaven, P. (2013). Description of the biogeochemical features of the subtropical southeastern Atlantic and the Southern Ocean south of South Africa during the austral summer of the International Polar Year. *European Geosciences Union*, *10*(10), pp.281–295.

Lin, C. T., Jickells, T. D., Baker, A. R., Marca, A., & Johnson, M. T. (2016). Aerosol isotopic ammonium signatures over the remote Atlantic Ocean. *Atmospheric Environment*, *133*, pp.165–169.

Lipschultz, F., (2008). Isotope tracer methods for studies of the marine nitrogen cycle. *Nitrogen in the Marine Environment*, 2nd Edition, Academic Press: Burlington, MA, USA, pp.1345-1384.

Llort, J., Lévy, M., Sallée, J.B., and Tagliabue, A., (2019). Nonmonotonic response of primary production and export to changes in mixed-layer depth in the Southern Ocean. *Geophysical Research Letters*, *46*(6), pp.3368-3377.

Longhurst, A. R. (1998). Ecological Geography of the Sea. Academic Press, San Diego, CA.

Lourey, M. J., Trull, T. W., and Sigman, D. M. (2003). Sensitivity of δ 15 N of nitrate, surface suspended and deep sinking particulate nitrogen to seasonal nitrate depletion in the Southern Ocean . *Global Biogeochemical Cycles*, *17*(3).

Lu, S., Liu, X., Liu, C., Cheng, G., and Shen, H., (2020). Influence of photoinhibition on nitrification by ammonia-oxidizing microorganisms in aquatic ecosystems. *Reviews in Environmental Science and Bio/Technology*, pp.1-12.

Lutjeharms, J. R. E., and Valentine, H. R. (1984). Southern ocean thermal fronts south of Africa. *Deep Sea Research Part A, Oceanographic Research Papers*, *31*(12), 1461–1475.

Macko, S.A., Estep, M.L.F., Engel, M.H., and Hare, P.E., (1986). Kinetic fractionation of stable nitrogen isotopes during amino acid transamination. *Geochimica et Cosmochimica Acta*, 50(10), pp.2143-2146.

Maldonado, M.T., Allen, A.E., Chong, J.S., Lin, K., Leus, D., Karpenko, N. and Harris, S.L., (2006). Copper-dependent iron transport in coastal and oceanic diatoms. *Limnology and oceanography*, 51(4), pp.1729-1743.

Marie, D., Partensky, F., Jacquet, S., and Vaulot, D., (1997). Enumeration and cell cycle analysis of natural populations of marine picoplankton by flow cytometry using the nucleic acid stain SYBR Green I. *Appl. Environ. Microbiol.*, *63*(1), pp.186-193.

Marie, D., Simon, N., and Vaulot, D., (2005). Phytoplankton cell counting by flow cytometry. *Algal culturing techniques*, *1*, pp.253-267.

Martin, J.H., Fitzwater, S.E., and Gordon, R.M., (1990). Iron deficiency limits phytoplankton growth in Antarctic waters. *Global Biogeochemical Cycles*, *4*(1), pp.5-12.

Martínez-García, A., Sigman, D.M., Ren, H., Anderson, R.F., Straub, M., Hodell, D.A., Jaccard, S.L., Eglinton, T.I., & Haug, G.H., (2014). Iron fertilization of the Subantarctic Ocean during the last ice age. *Science*, 343(6177), pp.1347-1350.

Mayzaud, P., Razouls, S., Errhif, A., Tirelli, V. and Labat, J.P., (2002). Feeding, respiration and egg production rates of copepods during austral spring in the Indian sector of the Antarctic Ocean: role of the zooplankton community in carbon transformation. *Deep Sea Research Part I: Oceanographic Research Papers*, 49(6), pp.1027-1048.

McIlvin, M.R. and Altabet, M.A., (2005). Chemical conversion of nitrate and nitrite to nitrous oxide for nitrogen and oxygen isotopic analysis in freshwater and seawater. *Analytical Chemistry*, 77(17), pp.5589-5595.

McIlvin, M.R., and Casciotti, K.L., (2011). Technical updates to the bacterial method for nitrate isotopic analyses. *Analytical Chemistry*, 83(5), pp.1850-1856.

Mdutyana, M., Thomalla, S.J., Philibert, R., Ward, B.B., and Fawcett, S.E., (2020). The seasonal cycle of nitrogen uptake and nitrification in the Atlantic sector of the Southern Ocean. *Global Biogeochemical Cycles*, *34*(7), p.e2019GB006363.

Mdutyana, M., (2021). Mixed layer nitrogen cycling in the Southern Ocean: seasonality, kinetics, and biogeochemical implications. (PhD dissertation, University of Cape Town).

Mei, Z.P., Finkel, Z.V., and Irwin, A.J., (2009). Light and nutrient availability affect the size-scaling of growth in phytoplankton. *Journal of theoretical biology*, *259*(3), pp.582-588.

Mengesha, S., Dehairs, F., Fiala, M., Elskens, M., and Goeyens, L. (1998). Seasonal variation of phytoplankton community structure and nitrogen uptake regime in the Indian Sector of the Southern Ocean. *Polar Biology*, *20*(4), pp.259–272.

Möbius, J., (2013). Isotope fractionation during nitrogen remineralization (ammonification): Implications for nitrogen isotope biogeochemistry. *Geochimica et Cosmochimica Acta*, *105*, pp.422-432.

Mongin, M., Nelson, D.M., Pondaven, P., & Tréguer, P., (2006). Simulation of upper-ocean biogeochemistry with a flexible-composition phytoplankton model: C, N and Si cycling and Fe limitation in the Southern Ocean. *Deep Sea Research Part II: Topical Studies in Oceanography*, 53(5-7), pp.601-619.

Mongwe, N., Vichi, M. and Monteiro, P., (2018). The seasonal cycle of pCO 2 and CO 2 fluxes in the Southern Ocean: diagnosing anomalies in CMIP5 Earth system models. *Biogeosciences*, 15(9), pp.2851-2872.

Moore, J.K. and Abbott, M.R., (2000). Phytoplankton chlorophyll distributions and primary production in the Southern Ocean. *Journal of Geophysical Research: Oceans*, *105*(C12), pp.28709-28722.

Mordy, C.W., Penny, D.M. and Sullivan, C.W., (1995). Spatial distribution of bacterioplankton biomass and production in the marginal ice-edge zone of the Weddell-Scotia Sea during austral winter. *Marine Ecology Progress Series*, *122*, pp.9-19.

Morel, F.M., Hudson, R.J., and Price, N.M., (1991). Limitation of productivity by trace metals in the sea. *Limnology and Oceanography*, 36(8), pp.1742-1755.

Mtshali, T.N., van Horsten, N.R., Thomalla, S.J., Ryan-Keogh, T.J., Nicholson, S.A., Roychoudhury, A.N., Bucciarelli, E., Sarthou, G., Tagliabue, A. and Monteiro, P.M., (2019). Seasonal depletion of the dissolved iron reservoirs in the sub-Antarctic zone of the Southern Atlantic Ocean. *Geophysical Research Letters*, *46*(8), pp.4386-4395.

Munk, W.H., and Riley, G., (1952). Absorption of nutrients by aquatic plants. *Journal of Marine Research,* 11, pp. 215-240.

Murphy, J., and Riley, J.P., (1962). A modified single solution method for the determination of phosphate in natural waters. *Analytica chimica acta*, *27*, pp.31-36.

Nelson, D.M., Brzezinski, M.A., Sigmon, D.E. and Franck, V.M., (2001). A seasonal progression of Si limitation in the Pacific sector of the Southern Ocean. *Deep Sea Research Part II: Topical Studies in Oceanography*, *48*(19-20), pp.3973-3995.

Nicholson, S.A., Lévy, M., Jouanno, J., Capet, X., Swart, S. and Monteiro, P.M., (2019). Iron supply pathways between the surface and subsurface waters of the Southern Ocean: from winter entrainment to summer storms. *Geophysical Research Letters*, 46(24), pp.14567-14575.

Olson, R.J. (1981). Differential photoinhibition of marine nitrifying bacteria: a possible mechanism for the formation of the primary nitrite maximum.

Orsi, A. H., Whitworth, T., and Nowlin, W. D. (1995). On the meridional extent and fronts of the Antarctic Circumpolar Current. *Deep-Sea Research Part I*, *42*(5), pp.641–673.

Owens, N.J.P., Priddle, J. and Whitehouse, M.J., (1991). Variations in phytoplanktonic nitrogen assimilation around South Georgia and in the Bransfield Strait (Southern Ocean). *Marine Chemistry*, 35(1-4), pp.287-304.

Pachiadaki, M.G., Sintes, E., Bergauer, K., Brown, J.M., Record, N.R., Swan, B.K., Mathyer, M.E., Hallam, S.J., Lopez-Garcia, P., Takaki, Y. and Nunoura, T., (2017). Major role of nitrite-oxidizing bacteria in dark ocean carbon fixation. *Science*, *358*(6366), pp.1046-1051.

Painter, S.C., Patey, M.D., Tarran, G.A. and Torres-Valdés, S., (2014). Picoeukaryote distribution in relation to nitrate uptake in the oceanic nitracline. *Aquatic Microbial Ecology*, 72(3), pp.195-213.

Palenik, B., Brahamsha, B., Larimer, F. W., Land, M., Hauser, L., Chain, P., Lamerdin, J., Regala, W., Allen, E. E., McCarren, J., Paulsen, I., Dufresne, A., Partensky, F., Webb, E. A., and Waterbury, J., (2003). The genome of a motile marine Synechococcus. *Nature*, *424*(6952), 1037–1042.

Paulot, F., Jacob, D. J., Johnson, M. T., Bell, T. G., Baker, A. R., Keene, W. C., Lima, I. D., Doney, S. C., and Stock, C. A., (2015). Global oceanic emission of ammonia: Constraints from seawater and atmospheric observations. *Global Biogeochemical Cycles*, *29*(8), pp.1165–1178.

Pausch, F., Bischof, K. and Trimborn, S., (2019). Iron and manganese co-limit growth of the Southern Ocean diatom Chaetoceros debilis. *Plos one*, *14*(9), p.e0221959.

Pearce, I., Davidson, A. T., Thomson, P. G., Wright, S., and van den Enden, R. (2010). Marine microbial ecology off East Antarctica (30 - 80°E): Rates of bacterial and phytoplankton growth and grazing by heterotrophic protists. *Deep-Sea Research Part II: Topical Studies in Oceanography*, 57(9–10), 849–862.

Peng, X., Fuchsman, C.A., Jayakumar, A., Oleynik, S., Martens-Habbena, W., Devol, A.H. and Ward, B.B., (2015). Ammonia and nitrite oxidation in the Eastern Tropical North Pacific. *Global Biogeochemical Cycles*, *29*(12), pp.2034-2049.

Philibert, R., Waldron, H. and Clark, D., (2015). A geographical and seasonal comparison of nitrogen uptake by phytoplankton in the Southern Ocean. *Ocean Science*, *11*(2).

Plate, T., and Heiberger, R., (2019). abind: Combine multi-dimensional arrays. R package version 1.1. https://cran.r-project.org/web/packages/abind

Pomeroy, L. R., and Wiebe, W. J. (2001). Temperature and substrates as interactive limiting factors for marine heterotrophic bacteria. *Aquatic Microbial Ecology*, *23*(2), pp.187–204.

Popp, B.N., Trull, T., Kenig, F., Wakeham, S.G., Rust, T.M., Tilbrook, B., Griffiths, B., Wright, S.W., Marchant, H.J., Bidigare, R.R., and Laws, E.A., (1999). Controls on the carbon isotopic composition of Southern Ocean phytoplankton. *Global Biogeochemical Cycles*, 13(4), pp.827-843.

Prézelin, B.B., Hofmann, E.E., Mengelt, C. and Klinck, J.M., (2000). The linkage between Upper Circumpolar Deep Water (UCDW) and phytoplankton assemblages on the west Antarctic Peninsula continental shelf. *Journal of Marine Research*, 58(2), pp.165-202.

Price, N.M., Ahner, B.A. and Morel, F.M., (1994). The equatorial Pacific Ocean: Grazer-controlled phytoplankton populations in an iron-limited ecosystem 1. *Limnology and Oceanography*, 39(3), pp.520-534.

Primeau, F. W., Holzer, M., and DeVries, T. (2013). Southern Ocean nutrient trapping and the efficiency of the biological pump. *Journal of Geophysical Research: Oceans*, *118*(5), pp.2547–2564.

R Core Team (2020). R: A language and environment for statistical computing. R Foundation for Statistical Computing, Vienna, Austria. URL https://www.R-project.org/.

Raven, J.A., (1988). The iron and molybdenum use efficiencies of plant growth with different energy, carbon and nitrogen sources. *New Phytologist*, *109*(3), pp.279-287.

Reay, D. S., Priddle, J., Nedwell, D. B., Whitehouse, M. J., Ellis-Evans, J. C., Deubert, C., and Connelly, D. P. (2001). Regulation by low temperature of phytoplankton growth and nutrient uptake in the Southern Ocean. *Marine Ecology Progress Series*, *219*(1990), pp.51–64.

Rees, A., Woodward, M. and Joint, I., (1999). Measurement of nitrate and ammonium uptake at ambient concentrations in oligotrophic waters of the North-East Atlantic Ocean. *Marine Ecology Progress Series*, 187, pp.295-300.

Rembauville, M., Briggs, N., Ardyna, M., Uitz, J., Catala, P., Penkerc'h, C., Poteau, A., Claustre, H., and Blain, S., (2017). Plankton assemblage estimated with BGC-Argo floats in the Southern Ocean: Implications for seasonal successions and particle export. *Journal of Geophysical Research: Oceans*, *122*(10), pp.8278-8292.

Ren, H., Sigman, D.M., Thunell, R.C. and Prokopenko, M.G., (2012). Nitrogen isotopic composition of planktonic foraminifera from the modern ocean and recent sediments. *Limnology and Oceanography*, 57(4), pp.1011-1024.

Revilla, M., Alexander, J., and Glibert, P.M., (2005). Urea analysis in coastal waters: comparison of enzymatic and direct methods. *Limnology and Oceanography: Methods*, *3*(7), pp.290-299.

Richardson, T.L. and Jackson, G.A., (2007). Small phytoplankton and carbon export from the surface ocean. *Science*, 315(5813), pp.838-840.

Rintoul, S.R., and Trull, T.W., (2001). Seasonal evolution of the mixed layer in the Subantarctic Zone south of Australia. *Journal of Geophysical Research: Oceans*, *106*(C12), pp.31447-31462.

Robinson, R.S., Jones, C.A., Kelly, R.P., Love, A., Closset, I., Rafter, P.A. and Brzezinski, M., (2020). A Test of the Diatom-Bound Paleoproxy: Tracing the Isotopic Composition of Nutrient-Nitrogen Into Southern Ocean Particles and Sediments. *Global Biogeochemical Cycles*, 34(10), p.e2019GB006508.

Rodrigues, R.M., and Williams, P.J.L.B., (2001). Heterotrophic bacterial utilization of nitrogenous and nonnitrogenous substrates, determined from ammonia and oxygen fluxes. *Limnology and Oceanography*, 46(7), pp.1675-1683.

Sallée, J.B., Speer, K.G. and Rintoul, S.R., (2010). Zonally asymmetric response of the Southern Ocean mixed-layer depth to the Southern Annular Mode. *Nature Geoscience*, 3(4), pp.273-279.

Sambrotto, R.N. and Mace, B.J., (2000). Coupling of biological and physical regimes across the Antarctic Polar Front as reflected by nitrogen production and recycling. *Deep Sea Research Part II: Topical Studies in Oceanography*, 47(15-16), pp.3339-3367.

Santoro, A.E., Sakamoto, C.M., Smith, J.M., Plant, J.N., Gehman, A.L., Worden, A.Z., Johnson, K.S., Francis, C.A. and Casciotti, K.L., (2013). Measurements of nitrite production in and around the primary nitrite maximum in the central California Current. *Biogeosciences*, 10(11), pp.7395-7410.

Sarmiento, J.L., and Orr, J.C., (1991). Three-dimensional simulations of the impact of Southern Ocean nutrient depletion on atmospheric CO2 and ocean chemistry. *Limnology and Oceanography*, 36(8), pp.1928-1950.

Sarmiento, J.L., and Toggweiler, J.R., (1984). A new model for the role of the oceans in determining atmospheric pCO2. *Nature*, 308(5960), pp.621-624.

Sarmiento, J. L., Gruber, N., Brzezinski, M. A., and Dunne, J. P. (2004). High-latitude controls of thermocline nutrients and low latitude biological productivity. *Nature*, *427*(6969), pp.56–60.

Savoye, N., Dehairs, F., Elskens, M., Cardinal, D., Kopczyńska, E.E., Trull, T.W., Wright, S., Baeyens, W., and Griffiths, F.B., (2004). Regional variation of spring N-uptake and new production in the Southern Ocean. *Geophysical Research Letters*, 31(3).

Schaafsma, F. L., Cherel, Y., Flores, H., van Franeker, J. A., Lea, M. A., Raymond, B., and van de Putte, A. P. (2018). Review: the energetic value of zooplankton and nekton species of the Southern Ocean. *Marine Biology*, 165(8), pp. 1–35.

Scharek, R., Smetacek, V., Fahrbach, E., Gordon, L.I., Rohardt, G., and Moore, S., (1994). The transition from winter to early spring in the eastern Weddell Sea, Antarctica: plankton biomass and composition in relation to hydrography and nutrients. *Deep Sea Research Part I: Oceanographic Research Papers*, *41*(8), pp.1231-1250.

Schön, G. H., and Engel, H. (1962). Der Einflußdes Lichtes auf Nitrosomonas europaea Win. *Archiv Für Mikrobiologie*, *42*(4), pp.415–428.

Sedwick, P. N., Bowie, A. R., and Trull, T. W. (2008). Dissolved iron in the Australian sector of the Southern Ocean (CLIVAR SR3 section): Meridional and seasonal trends. *Deep-Sea Research Part I: Oceanographic Research Papers*, *55*(8), pp.911–925.

Semeneh, M., Dehairs, F., Elskens, M., Baumann, M. E. M., Kopczynska, E. E., Lancelot, C., and Goeyens, L. (1998). Nitrogen uptake regime and phytoplankton community structure in the Atlantic and Indian sectors of the Southern Ocean. *Journal of Marine Systems*, *17*(1–4), pp.159–177.

Serebrennikova, Y. M., and Fanning, K. A. (2004). Nutrients in the Southern Ocean GLOBEC region: Variations, water circulation, and cycling. *Deep-Sea Research Part II: Topical Studies in Oceanography*, *51*(17–19), pp.1981–2002.

Shadwick, E.H., Trull, T.W., Tilbrook, B., Sutton, A.J., Schulz, E., and Sabine, C.L., (2015). Seasonality of biological and physical controls on surface ocean CO2 from hourly observations at the Southern Ocean Time Series site south of Australia. *Global Biogeochemical Cycles*, *29*(2), pp.223-238.

Shafiee, R.T., Snow, J.T., Zhang, Q., and Rickaby, R.E., (2019). Iron requirements and uptake strategies of the globally abundant marine ammonia-oxidising archaeon, Nitrosopumilus maritimus SCM1. *The ISME journal*, *13*(9), pp.2295-2305.

Shiozaki, T., Fujiwara, A., Ijichi, M., Harada, N., Nishino, S., Nishi, S., Nagata, T. and Hamasaki, K., (2018). Diazotroph community structure and the role of nitrogen fixation in the nitrogen cycle in the Chukchi Sea (western Arctic Ocean). *Limnology and Oceanography*, 63(5), pp.2191-2205.

Sigman, D. M., Altabet, M. A., McCorkle, D. C., Francois, R., and Fischer, G. (1999). The $\delta\,^{15}N$ of nitrate in the southern ocean: Consumption of nitrate in surface waters. *Global Biogeochemical Cycles*, *13*(4), pp.1149–1166.

Sigman, D.M. and Boyle, E.A., (2000). Glacial/interglacial variations in atmospheric carbon dioxide. *Nature*, *407*(6806), pp.859-869.

Silfer, J.A., Engel, M.H. and Macko, S.A., (1992). Kinetic fractionation of stable carbon and nitrogen isotopes during peptide bond hydrolysis: experimental evidence and geochemical implications. *Chemical Geology: Isotope Geoscience section*, 101(3-4), pp.211-221.

Sipler, R.E. and Bronk, D.A., (2015). Dynamics of dissolved organic nitrogen. *Biogeochemistry of marine dissolved organic matte*r, pp.127-232.

Smart, S. M., Fawcett, S. E., Thomalla, S. J., Weigand, M. A., Reason, C. J. C., and Sigman, D. M. (2015). Isotopic evidence for nitrification in the Antarctic winter mixed layer. *Global Biogeochemical Cycles*, *29*(4), 427–445.

Smart, S.M., Fawcett, S.E., Ren, H., Schiebel, R., Tompkins, E.M., Martínez-García, A., Stirnimann, L., Roychoudhury, A., Haug, G.H. and Sigman, D.M., (2020). The Nitrogen Isotopic Composition of Tissue and Shell-Bound Organic Matter

of Planktic Foraminifera in Southern Ocean Surface Waters. *Geochemistry, Geophysics, Geosystems*, 21(2), p.e2019GC008440.

Smith, J. M., Chavez, F. P., and Francis, C. A. (2014). Ammonium Uptake by Phytoplankton Regulates Nitrification in the Sunlit Ocean. *PLoS ONE*, *9*(9), e108173.

Smith Jr, W.O. and Harrison, W.G., (1991). New production in polar regions: the role of environmental controls. *Deep Sea Research Part A. Oceanographic Research Papers*, 38(12), pp.1463-1479.

Smith Jr, W.O. and Lancelot, C., (2004). Bottom-up versus top-down control in phytoplankton of the Southern Ocean. *Antarctic Science*, *16*(4), p.531.

Smith Jr, W.O., Marra, J., Hiscock, M.R. and Barber, R.T., (2000). The seasonal cycle of phytoplankton biomass and primary productivity in the Ross Sea, Antarctica. *Deep Sea Research Part II: Topical Studies in Oceanography*, *47*(15-16), pp.3119-3140.

Soares, M.A., Bhaskar, P.V., Naik, R.K., Dessai, D., George, J., Tiwari, M. and Anilkumar, N., (2015). Latitudinal δ13C and δ15N variations in particulate organic matter (POM) in surface waters from the Indian ocean sector of Southern Ocean and the Tropical Indian Ocean in 2012. *Deep Sea Research Part II: Topical Studies in Oceanography*, *118*, pp.186-196.

Sokolov, S. and Rintoul, S.R., (2007). On the relationship between fronts of the Antarctic Circumpolar Current and surface chlorophyll concentrations in the Southern Ocean. *Journal of Geophysical Research: Oceans*, *112*(C7).

Sosik, H.M. and Olson, R.J., (2002). Phytoplankton and iron limitation of photosynthetic efficiency in the Southern Ocean during late summer. *Deep Sea Research Part I: Oceanographic Research Papers*, *49*(7), pp.1195-1216.

Steinberg, D.K. and Saba, G.K., (2008). Nitrogen consumption and metabolism in marine zooplankton. In *Nitrogen in the marine environment* (pp. 1135-1196). Elsevier Inc.

Strickland, J.D.H. and Parsons, T.R., (1972). A practical handbook of seawater analysis.

Strzepek, R.F., Boyd, P.W. and Sunda, W.G., (2019). Photosynthetic adaptation to low iron, light, and temperature in Southern Ocean phytoplankton. *Proceedings of the National Academy of Sciences*, 116(10), pp.4388-4393.

Studer, A.S., Sigman, D.M., Martínez-García, A., Benz, V., Winckler, G., Kuhn, G., Esper, O., Lamy, F., Jaccard, S.L., Wacker, L. and Oleynik, S., (2015). Antarctic Zone nutrient conditions during the last two glacial cycles. *Paleoceanography*, 30(7), pp.845-862.

Sunda, W.G. and Huntsman, S.A., (1997). Interrelated influence of iron, light and cell size on marine phytoplankton growth. Nature, 390(6658), pp.389-392.

Tagliabue, A., Mtshali, T., Aumont, O., Bowie, A.R., Klunder, M.B., Roychoudhury, A.N. and Swart, S., (2012). A global compilation of dissolved iron measurements: focus on distributions and processes in the Southern Ocean. *Biogeosciences*, 9(6), pp.2333-2349.

Tagliabue, A., Sallée, J.B., Bowie, A.R., Lévy, M., Swart, S., and Boyd, P.W., (2014). Surface-water iron supplies in the Southern Ocean sustained by deep winter mixing. *Nature Geoscience*, *7*(4), pp.314-320.

Takao, S., Hirawake, T., Wright, S.W., and Suzuki, K., (2012). Variations of net primary productivity and phytoplankton community composition in the Indian sector of the Southern Ocean as estimated from ocean color remote sensing data. *Biogeosciences*, *9*(10), pp.3875-3890.

Talmy, D., Martiny, A.C., Hill, C., Hickman, A.E., and Follows, M.J., (2016). Microzooplankton regulation of surface ocean POC: PON ratios. *Global Biogeochemical Cycles*, 30(2), pp.311-332.

Tevlin, A.G., and Murphy, J.G., (2019). Atmospheric Ammonia: Measurements, Modeling, and Chemistry–Climate Interactions. *Advances In Atmospheric Chemistry-Volume 2: Organic Oxidation And Multiphase Chemistry*, *2*, p.1.

Thomalla, S.J., Waldron, H.N., Lucas, M.I., Read, J.F., Ansorge, I.J., and Pakhomov, E., (2011). Phytoplankton distribution and nitrogen dynamics in the southwest indian subtropical gyre and Southern Ocean waters. *Ocean Science*, *7*(1), pp.113-127.

Tilzer, M.M., and Dubinsky, Z., (1987). Effects of temperature and day length on the mass balance of Antarctic phytoplankton. *Polar Biology*, 7(1), pp.35-42.

Timmermans, K.R., Van Leeuwe, M.A., De Jong, J.T.M., McKay, R.M.L., Nolting, R.F., Witte, H.J., Van Ooyen, J., Swagerman, M.J.W., Kloosterhuis, H. and De Baar, H.J., (1998). Iron stress in the Pacific region of the Southern Ocean: evidence from enrichment bioassays. *Marine Ecology Progress Series*, *166*, pp.27-41.

Tolar, B.B., Ross, M.J., Wallsgrove, N.J., Liu, Q., Aluwihare, L.I., Popp, B.N., and Hollibaugh, J.T. (2016). Contribution of ammonia oxidation to chemoautotrophy in Antarctic coastal waters. *ISME Journal*, *10*(11), pp.2605–2619.

Tréguer, P. and Jacques, G., (1992). Review Dynamics of nutrients and phytoplankton, and fluxes of carbon, nitrogen and silicon in the Antarctic Ocean. In *Weddell Sea Ecology* (pp. 149-162). Springer, Berlin, Heidelberg.

Treibergs, L.A., Fawcett, S.E., Lomas, M.W. and Sigman, D.M., (2014). Nitrogen isotopic response of prokaryotic and eukaryotic phytoplankton to nitrate availability in Sargasso Sea surface waters. *Limnology and Oceanography*, 59(3), pp.972-985.

Trull, T.W., Davies, D. and Casciotti, K., (2008). Insights into nutrient assimilation and export in naturally iron-fertilized waters of the Southern Ocean from nitrogen, carbon and oxygen isotopes. *Deep Sea Research Part II: Topical Studies in Oceanography*, *55*(5-7), pp.820-840.

Tupas, L., & Koike, I. (1990). Amino acid and ammonium utilization by heterotrophic marine bacteria grown in enriched seawater. *Limnology and Oceanography*, 35(5), 1145–1155.

Utermöhl, H., (1958). Zur vervollkommnung der quantitativen phytoplankton-methodik: mit 1 Tabelle und 15 abbildungen im Text und auf 1 Tafel. *Internationale Vereinigung für theoretische und angewandte Limnologie: Mitteilungen*, *9*(1), pp.1-38.

Vaulot, D., Courties, C. and Partensky, F., (1989). A simple method to preserve oceanic phytoplankton for flow cytometric analyses. *Cytometry: The Journal of the International Society for Analytical Cytology*, *10*(5), pp.629-635.

Venkataramana, V., Anilkumar, N., Naik, R.K., Mishra, R.K. and Sabu, P., (2019). Temperature and phytoplankton size class biomass drives the zooplankton food web dynamics in the Indian Ocean sector of the Southern Ocean. *Polar Biology*, *42*(4), pp.823-829.

Viljoen, J.J., Weir, I., Fietz, S., Cloete, R., Loock, J., Philibert, R. and Roychoudhury, A.N., (2019). Links between the phytoplankton community composition and trace metal distribution in summer surface waters of the Atlantic southern ocean. *Frontiers in Marine Science*, *6*, p.295.

Volk, T., and Hoffert, M.I., (1985). Ocean carbon pumps: Analysis of relative strengths and efficiencies in ocean-driven atmospheric CO2 changes. *The carbon cycle and atmospheric CO2: natural variations Archean to present*, 32, pp.99-110.

Wadley, M.R., Jickells, T.D., and Heywood, K.J., (2014). The role of iron sources and transport for Southern Ocean productivity. *Deep Sea Research Part I: Oceanographic Research Papers*, *87*, pp.82-94.

Wan, X.S., Sheng, H.X., Dai, M., Zhang, Y., Shi, D., Trull, T.W., Zhu, Y., Lomas, M.W. and Kao, S.J., (2018). Ambient nitrate switches the ammonium consumption pathway in the euphotic ocean. *Nature communications*, *9*(1), pp.1-9.

Ward, B. B. (1985). Light and substrate concentration relationships with marine ammonium assimilation and oxidation rates. *Marine Chemistry*, *16*(4), pp.301–316.

Ward, B.B., (2005). Temporal variability in nitrification rates and related biogeochemical factors in Monterey Bay, California, USA. *Marine Ecology Progress Series*, *292*, pp.97-109.

Weber, L.H. and El-Sayed, S.Z., (1987). Contributions of the net, nano-and picoplankton to the phytoplankton standing crop and primary productivity in the Southern Ocean. *Journal of Plankton Research*, *9*(5), pp.973-994.

Wei, T., and Simko, V., (2017). R package "corrplot": Visualization of a Correlation Matrix (Version 0.84). Available from https://github.com/taiyun/corrplot

Weir, I., Fawcett, S., Smith, S., Walker, D., Bornman, T. and Fietz, S., (2020). Winter biogenic silica and diatom distributions in the Indian sector of the Southern Ocean. *Deep Sea Research Part I: Oceanographic Research Papers*, *166*, p.103421.

Welschmeyer, N.A., (1994). Fluorometric analysis of chlorophyll a in the presence of chlorophyll b and pheopigments. *Limnology and Oceanography*, *39*(8), pp.1985-1992.

Wickham H (2016). *ggplot2: Elegant Graphics for Data Analysis*. Springer-Verlag New York. ISBN 978-3-319-24277-4, https://ggplot2.tidyverse.org.

Xu, G., Chen, L., Zhang, M., Zhang, Y., Wang, J. and Lin, Q., (2019). Year-round records of bulk aerosol composition over the Zhongshan Station, Coastal East Antarctica. *Air Quality, Atmosphere & Health*, 12(3), pp.271-288.

Yool, A., Martin, A.P., Fernández, C., & Clark, D.R., (2007). The significance of nitrification for oceanic new production. *Nature*, 447(7147), pp.999-1002.

Yu G. (2019). shadowtext: Shadow Text Grob and Layer. R package version 0.0.7. https://CRAN.R-project.org/package=shadowtext

Zakem, E. J., Al-Haj, A., Church, M. J., Van Dijken, G. L., Dutkiewicz, S., Foster, S. Q., Fulweiler, R. W., Mills, M. M., and Follows, M. J. (2018). Ecological control of nitrite in the upper ocean. *Nature Communications*, *9*(1), pp.1–13.

Zhang, Y., Qin, W., Hou, L., Zakem, E.J., Wan, X., Zhao, Z., Liu, L., Hunt, K.A., Jiao, N., Kao, S.J. and Tang, K., (2020). Nitrifier adaptation to low energy flux controls inventory of reduced nitrogen in the dark ocean. *Proceedings of the National Academy of Sciences*, 117(9), pp.4823-4830.

Zhou, J., Delille, B., Kaartokallio, H., Kattner, G., Kuosa, H., Tison, J.L., Autio, R., Dieckmann, G.S., Evers, K.U., Jørgensen, L. and Kennedy, H., (2014). Physical and bacterial controls on inorganic nutrients and dissolved organic carbon during a sea ice growth and decay experiment. *Marine Chemistry*, 166, pp.59-69.

Figure and Table Captions

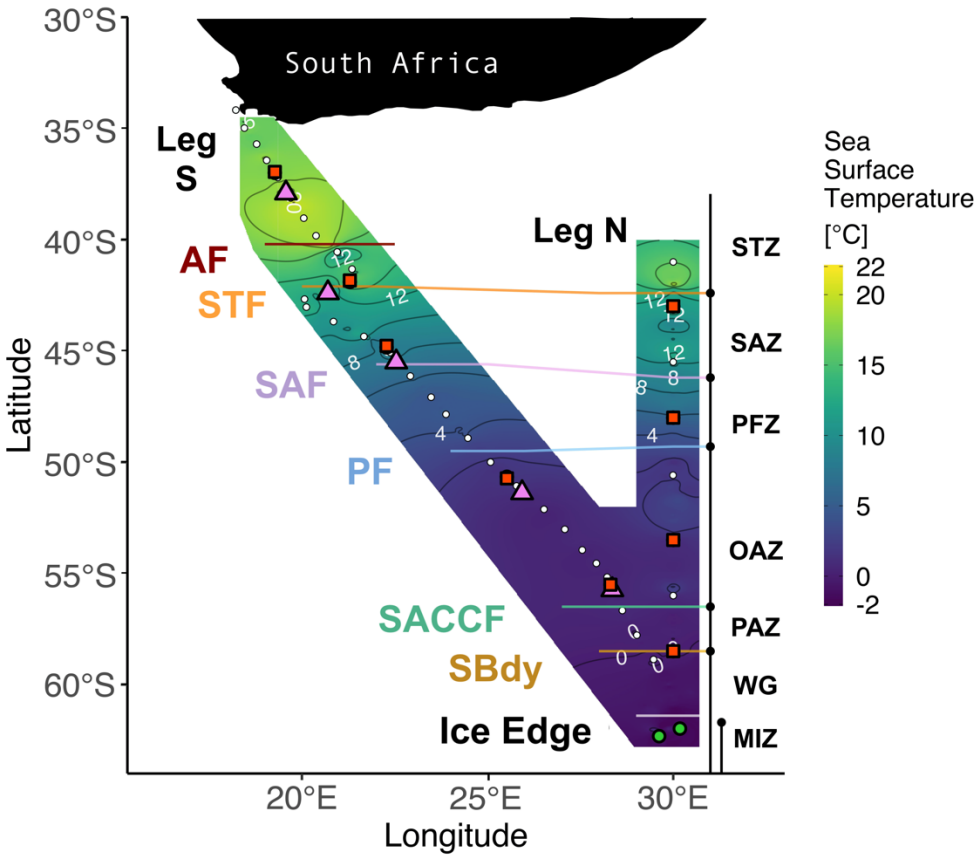

Figure 1: Winter 2017 cruise track overlaid on sea surface temperature (SST) measured by the hull-mounted thermosalinograph. The underway (Leg S) and CTD (Leg N) stations are indicated by white circles. Stations at which net primary production (NPP), nitrogen uptake, and ammonium oxidation experiments were conducted are denoted by red squares. The pink triangles indicate stations where only NPP experiments were conducted while the green circles show stations where only ammonium oxidation was measured. Solid lines indicate the positions of the fronts, identified from measurements of temperature and salinity. Abbreviations for fronts: AF – Agulhas Front (~40.2°S); STF – Subtropical Front (~42.1°S); SAF – Subantarctic Front (~45.6°S); PF – Polar Front (~49.5°S); SACCF – Southern Antarctic Circumpolar Current Front (~56.5°S); SBDY – Southern Boundary (~58.5°S). Abbreviations for zones: STZ – Subtropical Zone; SAZ – Subantarctic Zone; PFZ – Polar Frontal Zone; OAZ – Open Antarctic Zone; PAZ – Polar Antarctic Zone; WG – Weddell Gyre; MIZ – Marginal Ice Zone. Together, the OAZ and PAZ constitute the Antarctic Zone (AZ). See Text S1 for detailed definitions of the fronts and zones. Figure produced using the package ggplot2 (Wickham, 2016).

Table 1: Mean (± 1 SD) of surface ocean POC, PON, chl-a, and nutrient concentrations, cell abundances, and nutrient uptake rates measured in each zone of the Southern Ocean in winter 2017. Where no SD is given, only one sample was measured. The >0.3 µm and >2.7 µm size fractions are referred to as "bulk" and "nano+", respectively. "% of nano+" refers to the average relative contribution of the nano+ size fraction to total chl-a, POC, or PON, calculated for each station within a zone. The f-ratio including ρUrea

is only shown for zones where ρUrea was measured at all stations. "ND" indicates no data available. Abbreviations as in Figure 1.

	STZ	SAZ	PFZ	OAZ	PAZ
NH_4^+ (µM)	0.08±0.03	0.06±0.01	0.42±0.01	0.52±0.01	0.58±0.01
PO_4^{3-} (µM)	0.44±0.07	0.90±0.06	1.59±0.1	2.00±0.13	1.99±0.09
NO_3^- (µM)	3.6±0.2	10.5±0.5	21.5±0.2	26.7±0.4	27.5±0.4
$Si(OH)_4$ (µM)	2.6±0.1	2.5±1.8	6.6±0.1	40.3±0.5	45.0±0.8
NO_2^- (µM)	0.15±0.02	0.13±0.02	0.17±0.02	0.19±0.01	0.21±0.02
Urea (µM)	0.23±0.04	0.11±0.04	0.26±0.08	0.24	0.21±0.03
chl-a (bulk) (µg L^{-1})	0.65±0.08	0.43±0.05	0.35±0.03	0.25±0.02	0.21±0.00
chl-a (nano+) (µg L^{-1})	0.50±0.05	0.30±0.04	0.24±0.02	0.18±0.02	0.17±0.02
chl-a (pico) (µg L^{-1})	0.15±0.1	0.13±0.07	0.11±0.04	0.06±0.03	0.04±0.02
chl-a (% of nano+)	77.5±13.9	73.1±10.9	69.8±8.7	76.7±11.3	80.1±8.5
POC (bulk) (µM)	4.4±6.7	3.4±0.4	3.2±0.3	3.4±0.5	3.5+0.2
POC (nano+) (µM)	2.6±0.5	2.6±0.4	1.9±1.2	1.9±0.4	4.6
PON (bulk) (µM)	0.6±0.2	0.5±0.1	0.4±0.1	0.5±0.1	0.5±0.1
PON (nano+) (µM)	0.3±0.1	0.3±0.1	0.2±0.3	0.2±0.1	0.4±0.0
POC (% of nano+)	79.7±24.6	79.6±19.0	50.9±33.2	77.2±21.8	ND
PON (% of nano+)	69.0±31.9	67.1±17.2	53.8±24.1	67.0±21.9	51.1±24.7
POC:chl-a (g g^{-1})	103.0±22.1	102.5±14.4	122.5±11	234.1±29.2	219.3±1.0
POC:PON (M/M)	7.81±6.49	6.90±1.25	7.13±0.71	6.72±1.62	5.80±3.75
δ^{15}N-PON	1.4±0.9	1.2±1.0	0.3±0.5	-1.3±0.5	-1.3±0.4
NPP (bulk) (nM day^{-1})	497.1±42.4	277.5±21.3	289.7±19.2	85.3±26.1	27.7±0.2
NPP (nano+) (nM day^{-1})	384.7±29.7	178.2±23.4	193.5	49.6±5.0	ND
ρNH_4^+ (bulk) (nM day^{-1})	5.7±0.8	8.9±1.1	12.9±0.4	4.8±0.1	3.0±0.8
ρNH_4^+ (nano+) (nM day^{-1})	4.0±1.1	4.1±1.2	4.2±4.7	3.1±0.4	ND
ρNO_3^- (bulk) (nM day^{-1})	4.1±0.4	11.5±1.4	5.9±1	3.6±0.4	3.7±1.8
ρNO_3^- (nano+) (nM day^{-1})	3.4±0.3	6.6±0.4	4.3±0.4	2.6±0.8	2.7±1.2
ρUrea (bulk) (nM day^{-1})	7.5±0.6	6.9±0.3	6.5±1.0	2.1±0.3	0.6±0.01
ρUrea (nano+) (nM day^{-1})	4.9±0.3	3.8±0.2	4.0±0.6	1.3±0.2	0.7±0.4
f-ratio (bulk) (including ρUrea)	0.21±0.31	0.43±0.11	0.23±0.18	ND	0.51±0.53
f-ratio (bulk) (excluding ρUrea)	0.43±0.32	0.57±0.12	0.31±0.18	0.43±0.16	0.55±0.54
NH_4^+ox (nM day^{-1})	9.3±0.5	12.9±0.6	11.1	17.7±0.6	14.3±1.0
Total microplankton (cells mL^{-1})	13±11	5±3	9±3	6±6	4±2
Centric diatoms (cells mL^{-1})	<1	<1	<1	<1	1±2
Pennate diatoms (cells mL^{-1})	2±4	<1	2±1	2±3	<1
Dinoflagellates (cells mL^{-1})	7±6	4±0	6±2	3±2	2±0
Micro-zooplankton (cells mL^{-1})	4±3	<1	2±2	1±2	<1
Nanoeukaryotes (cells mL^{-1})	ND	2.2±1.4 E+03	1.5±0.7 E+03	1.6±0.7 E+03	1.4E+03
Picoeukaryotes (cells mL^{-1})	ND	4.5±2.9 E+03	4.9±3.7 E+03	1.5±0.5 E+03	8E+02
Synechococcus (cells mL^{-1})	ND	3.8±1.8 E+03	2.3±1.1 E+03	1.4±0.2 E+03	1E+03

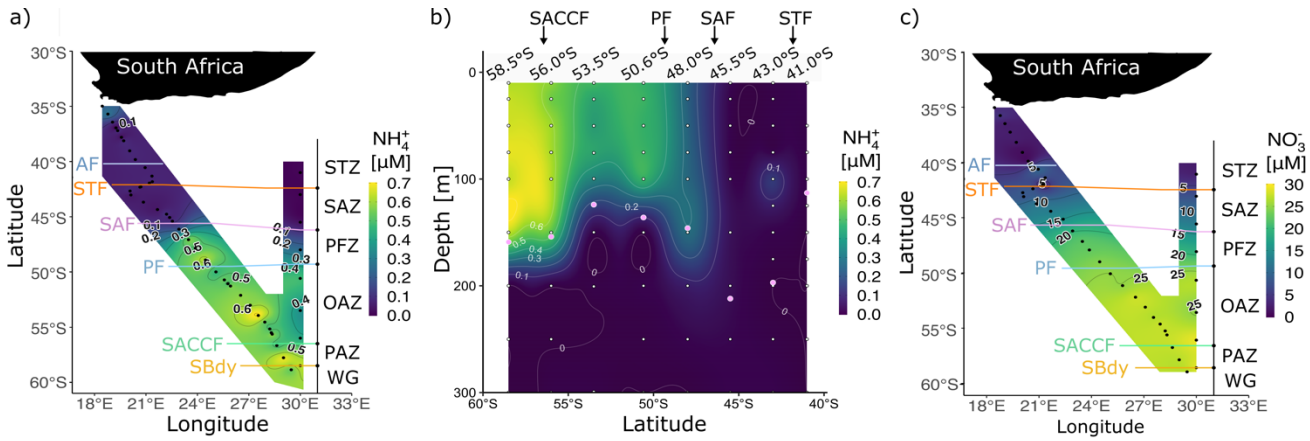

1522

1523 *Figure 2*: Concentrations of dissolved ammonium (NH_4^+) a) at the surface for Legs S and N and b) with
1524 depth (0-300 m) for Leg N, and c) concentrations of nitrate (NO_3^-) at the surface for Legs S and N. Pink
1525 circles in panel b show the mixed layer depth at the CTD stations. Abbreviations are as in Figure 1. Figure
1526 produced using the package ggplot2 (Wickham, 2016).

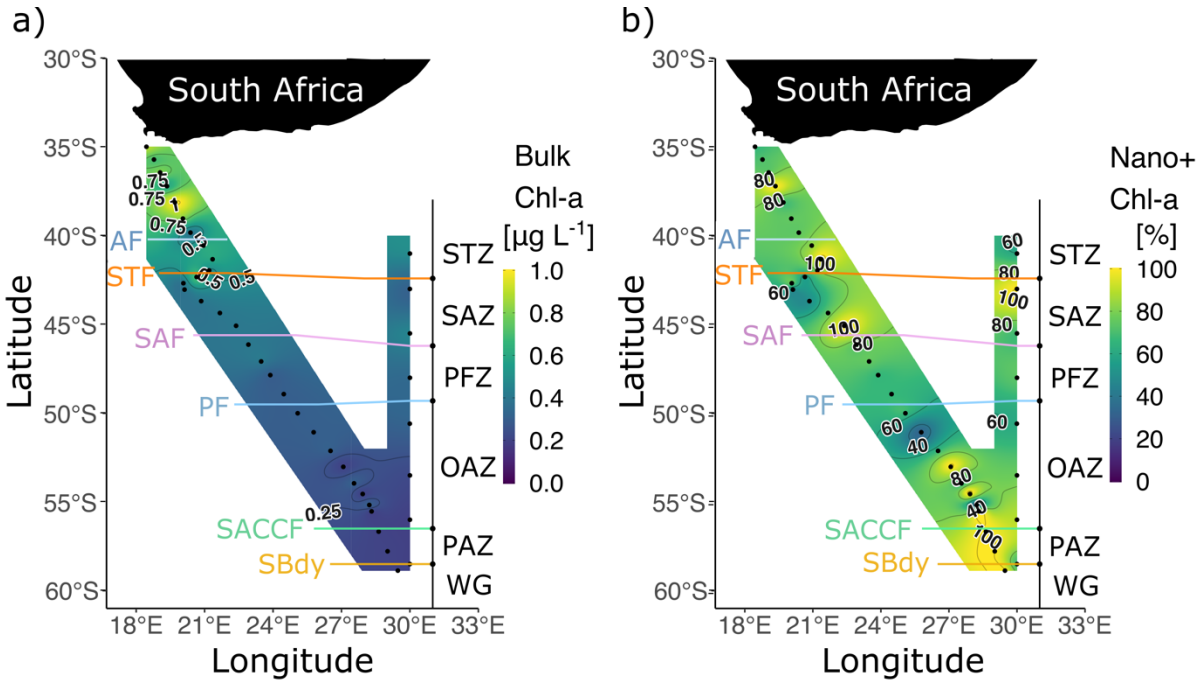

1527

1528 *Figure 3*: a) Bulk chlorophyll-a (chl-a) concentrations and b) the proportion of chlorophyll-a in the nano+
1529 size fraction at the surface for Legs S and N. Abbreviations are as in Figure 1. Figure produced using the
1530 package ggplot2 (Wickham, 2016).

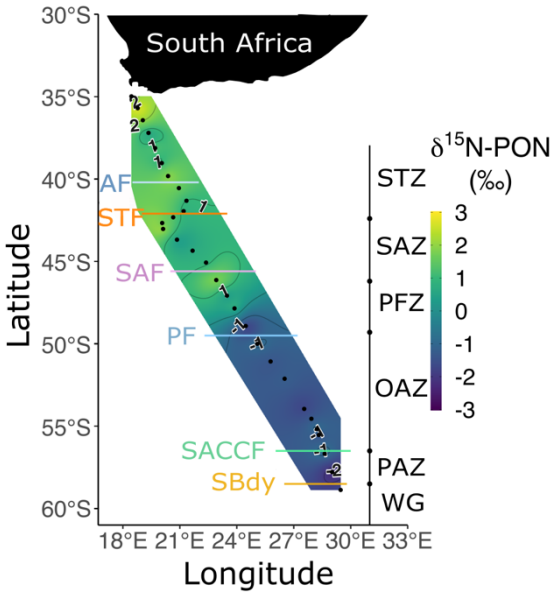

1531

1532 *Figure 4*: Bulk δ^{15}N-PON at the surface for Leg S in winter 2017. Two stations nearest South Africa at
1533 which biomass concentrations were extremely high have been excluded. Abbreviations are as in Figure
1534 1. Figure produced using the package ggplot2 (Wickham, 2016).

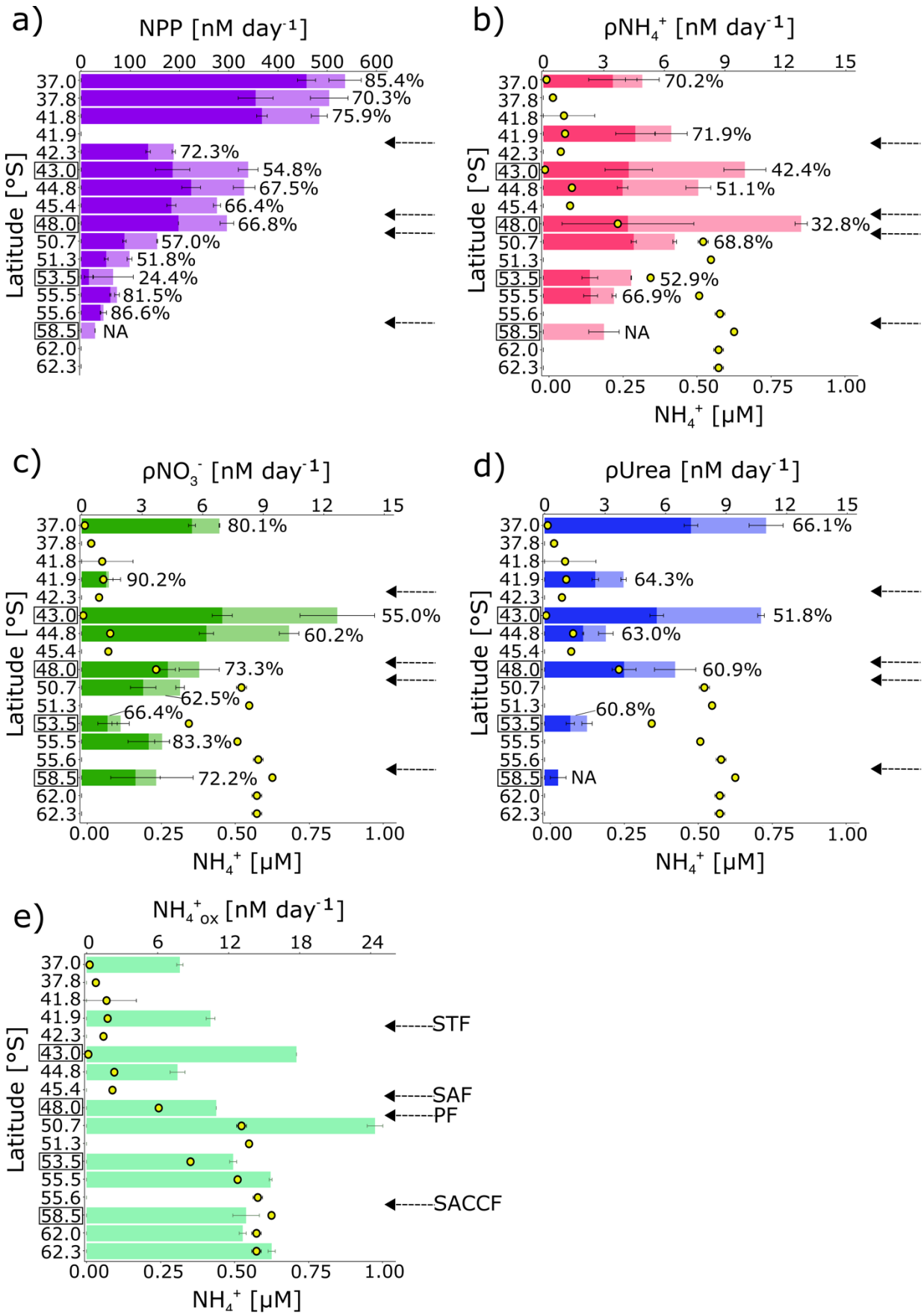

1535

1536 *Figure 5*: Surface rates of a) net primary production (NPP) and rates of b) ammonium (ρNH_4^+), c) nitrate
1537 (ρNO_3^-), and d) urea (ρUrea) uptake by the pico (light colours) and nano+ (dark colours) size fractions,
1538 with the full length of the bars indicating the bulk rates, and e) NH_4^+ oxidation. Error bars indicate ±1

standard deviation of duplicate experiments. The percentage of total NPP and N uptake attributable to the nano+ size fraction is written next to each bar in panels a-d. NPP and NH_4^+ uptake were not measured for the nano+ size fraction at 58.5°S, and urea uptake was not measured at 50.7°S and 55.5°S. Rates were not measured at the latitudes where no data are shown. In panels b-e, the surface NH_4^+ concentration at each station is shown by the yellow circles. Leg N stations (at which samples were collected from Niskin bottles fired at 10 m) are indicated by black boxes surrounding the latitude. By contrast, samples were collected at the Leg S stations (no square surrounding the latitude) from the ship's underway system (~7 m). Fronts are indicated with arrows (labeled in panel e), and abbreviations are as in Figure 1. Figure produced using the package ggplot2 (Wickham, 2016).

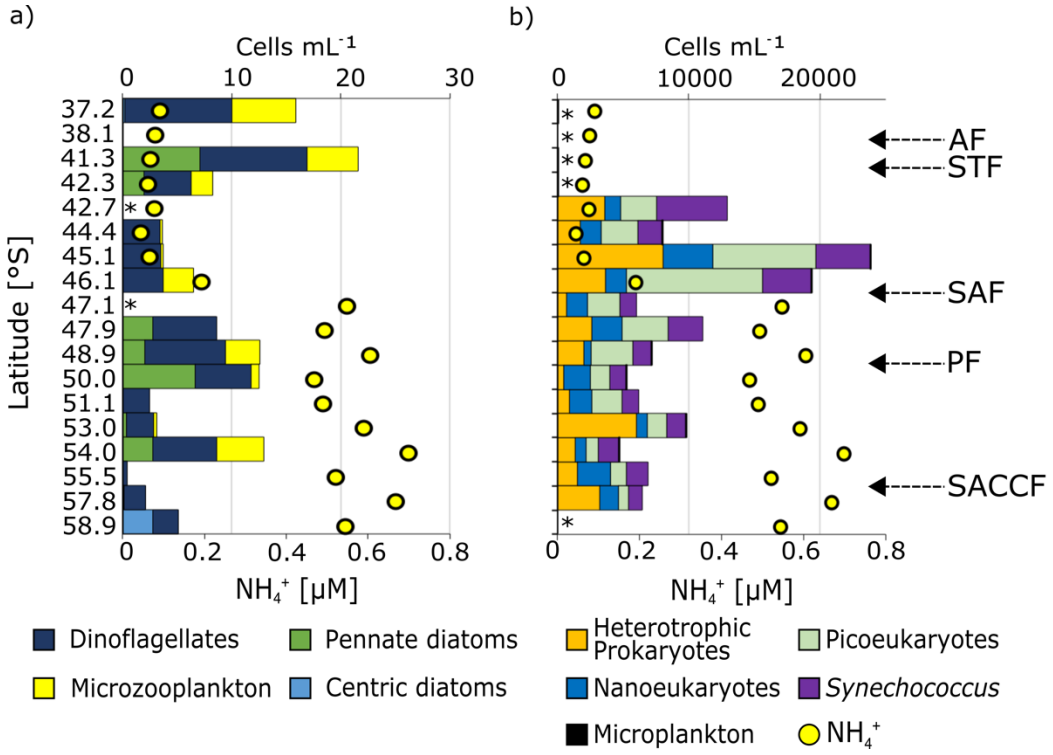

Figure 6: Surface community composition for a) plankton ≥15 µm (enumerated by microscopy) and b) the total community <15 µm (enumerated by flow cytometry). For context, the surface NH_4^+ concentration at each station is shown by the yellow circles. * indicates stations at which no measurements were made while the absence of a bar with no * indicates that no cells were detected. Note that the abundances shown on panel b (top x-axis) are >2 orders of magnitude greater than those shown in panel a. The "microplankton" shown in panel a are included on panel b (slim black bars) to illustrate the difference in abundance between the micro- and pico+nano populations. The frontal positions are indicated on panel b, with abbreviations as in Figure 1.

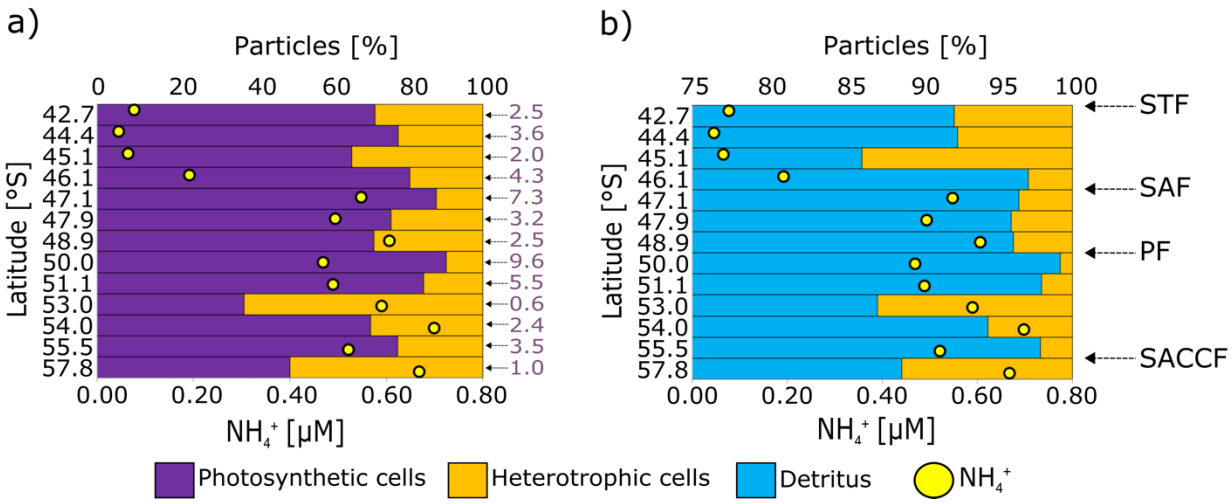

Figure 7: Relative abundances of a) total photosynthetic versus heterotrophic bacteria and b) detritus versus heterotrophic bacteria at the surface for Leg S. The surface NH_4^+ concentration at each station is indicated by the yellow dots. The values in maroon text on the right side of panel a are the photosynthetic-to-heterotrophic cell ratios. The upper x-axis in panel b begins at 75% in order to highlight the (much smaller) heterotrophic bacterial contribution to the summed detrital + heterotrophic particles. Frontal abbreviations are as in Figure 1.

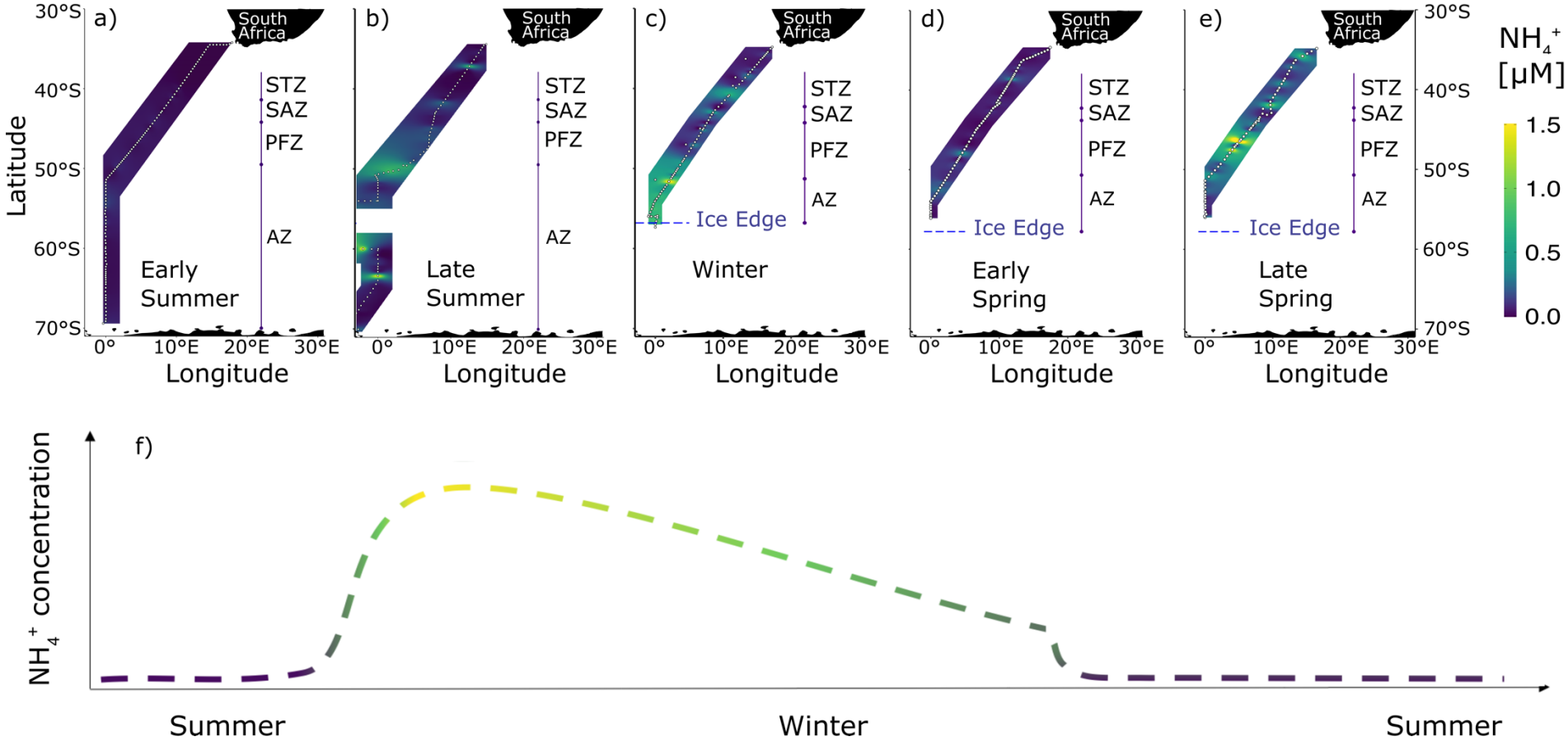

Figure 8: Surface concentrations of NH_4^+ across the eastern Atlantic sector of the Southern Ocean measured between December 2018 and November 2019. Five unique transects (additional to the winter 2017 dataset presented in Fig. 2a) are shown: a) early summer 2018, b) late summer 2019, c) winter 2019, d) early spring 2019, and e) late spring 2019. f) The proposed seasonal cycle of NH_4^+ concentrations in the mixed layer south of the Subantarctic Front. The colour gradient in panel f shows the transition between late summer and late winter. Panels a and b cover a latitudinal extent of 30-70°S, while panels c-e cover 30-60°S due to the presence of sea-ice. Abbreviations are as in Figure 1, with AZ referring to the combined OAZ and PAZ. Figure produced using the package ggplot2 (Wickham, 2016).

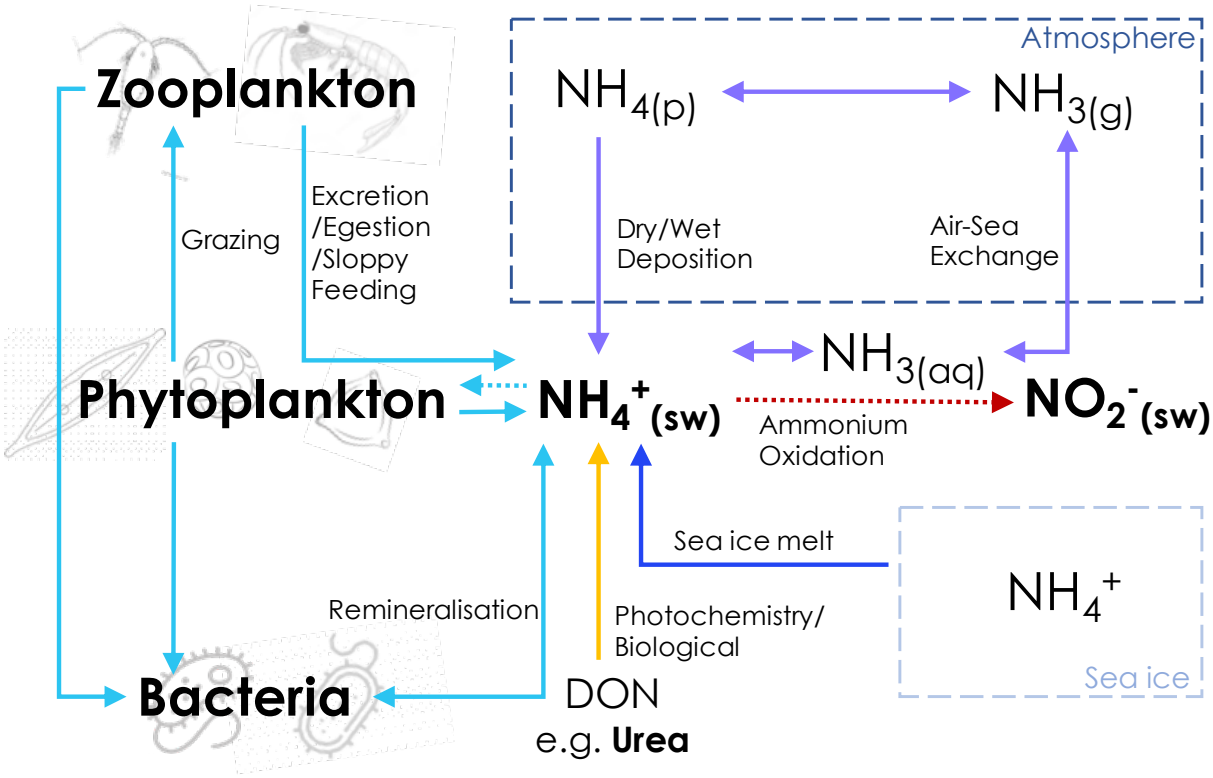

1565

1566 *Figure 9*: Schematic of the possible mixed-layer NH_4^+ assimilation and production pathways. Bold text
1567 indicates components of the NH_4^+ cycle that were directly measured in this study (seawater concentrations
1568 of NH_4^+, NO_2^-, and urea; phytoplankton, bacterial, and microzooplankton cell abundances), and dotted
1569 lines indicate processes for which we have direct rate measurements (phytoplankton uptake of NH_4^+;
1570 oxidation of NH_4^+ to NO_2^-). Dashed-line boxes represent the atmosphere and sea-ice, with all other
1571 processes occurring in the ocean. DON – dissolved organic nitrogen; $NH_{3(aq)}$ – aqueous (seawater)
1572 ammonia; $NH_{4(p)}$ – ammonium aerosols (including ammonium sulphate, ammonium bisulphate, and
1573 ammonium nitrate); $NH_{3(g)}$ – ammonia gas.